https://doi.org/10.5194/egusphere-2025-5562
Preprint. Discussion started: 17 February 2026

Interannual and Seasonal Evolution of Supraglacial Channel Networks on Nivlisen Ice Shelf, East Antarctica

Jiao Chen[1], Rebecca A. Hodge[1], Stewart S.R. Jamieson[1], Chris R. Stokes[1]

[1]Department of Geography, Durham University, Durham, DH1 3LE, UK

Correspondence to: Jiao Chen (jiao.chen@durham.ac.uk)

Abstract. Supraglacial channel networks (SCNs) represent critical components of the surface drainage system on Antarctic ice shelves, facilitating the redistribution of meltwater, including into and out of supraglacial lakes, potentially influencing ice-shelf stability. However, the seasonal and interannual variability in their spatial extent, structural evolution, and climatic sensitivity remain poorly quantified, particularly compared to observations of supraglacial lakes. In this study, we investigate the interannual evolution of SCNs on Nivlisen Ice Shelf in East Antarctica between 2017 and 2024 using Sentinel-2 and Landsat-8 satellite imagery, with a detailed seasonal analysis during the 2018-2019 melt season. Key metrics including surface water area, total channel length, number of SCNs, and the number of individual channels were derived to quantify the drainage evolution and system connectivity and complexity. We find significant interannual variability in SCN count (from 34 to 186) and total channel length (from 345 to 1275 km), with peak length of channels observed in 2018. During the 2018-2019 melt season SCNs progressively integrated and connected to form an efficient drainage system, which then fragmented towards the end of the melt season. We find that SCNs are strongly influenced by the ice shelf surface structures and ice surface undulations at a range of scales, with larger channels reforming in the same location. Correlation analysis shows that annual SCN evolution is tightly coupled to regional air temperature, with surface water extent and network connectivity strongly linked to reanalysis-based temperature outputs ($r > 0.9$, $p < 0.05$). Snow had variable effects, depending on its timing and how readily it could be melted. Our findings underscore the important dynamic nature of supraglacial channels in redistributing meltwater on Antarctic ice shelves.

https://doi.org/10.5194/egusphere-2025-5562
Preprint. Discussion started: 17 February 2026

1 Introduction

As climate warming accelerates, the Antarctic Ice Sheet (AIS), which contains approximately 30 million km^3 of ice, has lost mass at rates estimated at -127±23 Gt year^{-1} from 2002 to 2022 (Hanna et al., 2024). The floating ice shelves around the AIS, which hold back the grounded ice from further inland, are faced with potential threats from surface melt (Bell et al., 2018; Arthur et al., 2022; Tuckett et al., 2025). Indeed, surface water is more widespread across the AIS than previously assumed, and numerous supraglacial lakes (SGLs) and channels have been observed on Antarctic ice shelves during recent years (Langley et al., 2016; Lenaerts et al., 2017; Stokes et al., 2019; Tuckett et al., 2021; Arthur et al., 2022; Tuckett et al., 2025). For example, more than 65,000 SGLs (over 1300 km^2) have been observed around the margin of the East Antarctic Ice Sheet (EAIS) in the peak of the melt season in January 2017, and approximately 60 % of these lakes developed on ice shelves (Stokes et al. 2019). Meanwhile, Corr et al. (2022) identified 10,223 lakes (114.7 km^2) and 255 channels (4.7 km^2) on the West Antarctic Ice Sheet (WAIS) and Antarctic Peninsula (AP) during January 2017 from satellite imagery.

Supraglacial lakes can trigger the collapse of ice shelves by 'hydrofracturing', a process of meltwater-induced vertical fracture propagation, (Banwell et al., 2014; Dunmire et al., 2020). Primary mechanisms of hydrofracturing induced by SGLs include (1) stored meltwater in lakes that can fill and drain vertically through the pre-existing fractures (Van Der Veen, 2007); (2) clusters of multiple lakes rapidly increasing the local hydrostatic pressure leading to crack propagation (Banwell et al., 2013); and (3) surface meltwater percolating into the firn layer and refreezing, reducing its capacity to absorb water due to the reduction of pore space and promoting the formation of impermeable near-surface ice lenses (Vandecrux et al., 2020). Although some Antarctic ice shelves are already thought to be vulnerable to hydrofracturing (Alley et al., 2018; Arthur et al., 2022), future surface melt is expected to enhance the likelihood of ice shelf disintegration by progressively reducing their capacity to store or absorb surface meltwater (Bell et al., 2018).

The potential impacts of SGLs (e.g. via hydrofracturing) means that they have received considerable attention in Antarctica. In contrast, supraglacial channels have been relatively overlooked, despite playing a key role in controlling the storage and routing of meltwater between SGLs and across whole ice shelves (Pitcher and Smith, 2019; Chandler and Hubbard, 2023), including over substantial distances, e.g. over 120 km (Kingslake et al., 2017; Corr et al., 2022). Depending on the efficiency of the channel network, they can move meltwater away from some areas of the ice shelf while concentrating it in others, thereby modulating the formation and persistence of SGLs and the drainage of water into the firn. For example, recent satellite observations reveal that some lakes are connected to each other by channels, forming more efficient large-scale drainage networks and moving surface meltwater from higher to lower elevations (Kingslake et al., 2015; Yang et al., 2021; Chen et al., 2024). The efficiency and extent of meltwater routing through channels have important implications for ice shelf stability. Channels can both move water within ice shelves and even off the ice shelf, thereby mitigating any potential for widespread hydrofracturing (Bell et al., 2017). Indeed, Bell et al. (2017) observed a 130 m wide waterfall (discharge 259 to 806 m^3 s^{-1}) on the ice cliff of the Nansen Ice Shelf in the WAIS. As such, they found that active

https://doi.org/10.5194/egusphere-2025-5562
Preprint. Discussion started: 17 February 2026

drainage networks on Nansen Ice Shelf exported a large volume of water (0.04 km^3 to 0.56 km^3 in each melt season) off the ice surface through one waterfall between 2006 and 2015. The efficient export of surface meltwater on Nansen Ice Shelf highlights the potential capacity of channels to stabilize ice shelves by reducing the risk of damage related to extensive storage of meltwater (Bell et al., 2018), but such waterfalls have not been widely reported elsewhere in Antarctica and the prevalence and spatial extent of such drainage pathways remain poorly constrained.

Understanding the development of SCNs is therefore important because they can potentially increase the risk of ice shelf collapse (by focussing water in lakes and/or firn) or enhance ice shelf stability (by draining meltwater off the ice shelf). However, there are very few detailed studies of the size and connectivity of SCNs and how different types of systems might develop and under what conditions. To better understand the evolution of SCNs, it is important to conduct interannual and seasonal observations of their spatial and temporal extent across ice shelves. This paper aims to characterize and explain the evolution of supraglacial channels on Nivlisen Ice Shelf between 2017 and 2024. We map SCNs (drainage networks including both lakes and channels) from satellite imagery and track their spatio-temporal evolution over multiple melt seasons. The Nivlisen Ice Shelf has a multidecadal history of surface meltwater activity (Kingslake et al., 2015; Dell et al., 2020; Tuckett et al., 2025), making it an ideal site to: (1) quantify spatial and temporal variations in SCNs across seasonal to interannual scales; (2) observe changes on the inter-connectivity of SCNs; and (3) identify the dominant climate controls on the development of drainage systems.

2 Study area

The Nivlisen Ice Shelf (70°68' S,12°09' E) is located in Dronning Maud Land, East Antarctica, and has a surface area of 7600 km^2 mainly fed by the Potsdam Glacier (Fig. 1). The ice shelf thickness ranges from 700 m at the grounding line to 150 m at the ice cliff (Dell et al., 2020). The average ice velocity of the Nivlisen is around 80 m a^{-1} (Fig. 1b) which is relatively slow compared to other ice shelves in Dronning Maud Land (e.g. Roi Baudouin ice shelf flows up to 205 m a^{-1} at average) (Berger et al., 2016; Lindbäck et al., 2019). The surface conditions, including the firn and near-surface ice structures, differ significantly across Nivlisen Ice Shelf. A Blue Ice Area (BIA) extends beyond 100 km in the southeast direction and surrounds the exposed nunatak (called the Schirmacher Oasis) with an area of approximately 34 km^2 (Fig. 1c). North of this BIA, the ice shelf transitions into an accumulation zone, where the firn layer becomes thicker. According to Kingslake et al. (2015), there was large significant meltwater coverage nearly every summer over Nivlisen Ice Shelf during the past 20 years, and the extent of surface water showed significant seasonal and interannual variations, but these variations were not quantified.

https://doi.org/10.5194/egusphere-2025-5562
Preprint. Discussion started: 17 February 2026

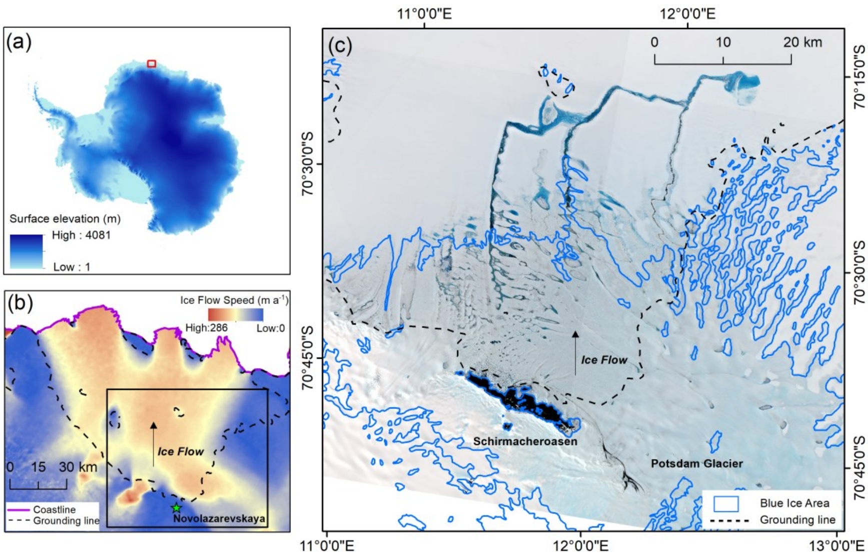

Figure 1: A map of the study area: (a) surface elevation of the Antarctica Ice Sheet and surrounding ice shelves from Bedmap2 (Fretwell et al., 2022), with red box indicating the location of Nivlisen Ice Shelf; (b) the ice flow speed, including the Novolazarevskaya Research Station, coastline and grounding line from Mouginot et al. (2017) and (c) SCNs on Nivlisen Ice Shelf on 26 January 2020. The solid blue lines delineate the BIA regions from Hui et al. (2014) . The boxes in (a) and (b) illustrate the study area extent. The base imagery of (c) is a mosaicked RGB Sentinel-2 image of Nivlisen Ice Shelf.

Previous work on Nivlisen Ice Shelf has documented a complex surface hydrological system (e.g., Kingslake et al., 2015; Dell et al., 2020; Arthur et al.,2022; Chen et al., 2025), but the research focus has varied, with few studies quantifying the interannual and seasonal evolution of the channel network in detail. Dell et al. (2020), Dirscherl et al. (2021), and Arthur et al. (2022) characterized SGLs, detailing their distribution, volume changes, and links to climatic factors, but limited attention was paid to the structure and evolution of the SCNs. Recent work by Tuckett et al. (2025) included both lakes and channels but with a focus very much on the total extent of meltwater, finding a moderate increase in annual surface meltwater area from 2006/7 to 2020/21. Some studies have considered water transfer through channels. Dell et al. (2020) used Landsat-8 and Sentinel-2 imagery to track surface meltwater on Nivlisen Ice Shelf during summer 2016-2017. They identified 1598 water bodies, which were classified as either circular or linear features. The total volume of surface meltwater peaked at 5.5×10^7 m^3 on 26 January 2017, and 63 % of the total meltwater was stored in two linear features following the surface slopes which extended up to 27 km in length. Kingslake et al. (2015) also highlighted supraglacial lake drainage through surface channels over extensive distances (over 70 km). This large-scale lateral water transfer may affect the structure and stability of Nivlisen Ice Shelf in the future, as lateral transfer can saturate firn, lower firn-air content, and promote ponding and hydrofracturing in otherwise colder

https://doi.org/10.5194/egusphere-2025-5562
Preprint. Discussion started: 17 February 2026

regions, with latent-heat release on refreezing further warming and weakening the ice shelf (Dell et al.,2020).

Subsequent detailed investigations have largely prioritised SGLs. Dirscherl et al. (2021) expanded the temporal scope (2015-2021) by using Sentinel-1/2 satellite imagery to map the SGLs on Nivlisen Ice Shelf, recording a maximum extent of 107 km^2 in early January 2019. Their analysis linked the formation of lakes to climatic factors (i.e., air temperature, solar radiation, wind conditions), and warned that repeated meltwater ponding and drainage may cause the destabilisation of ice shelves to occur sooner than expected. Arthur et al. (2022) quantified the SGLs around the EAIS during multiple melt seasons (2014-2020) from Landsat-8 imagery. Their results demonstrated that the interannual variability of the SGL volume on Nivlisen was one of the highest in East Antarctica (peaking at 144 ×106 m^3 in summer of 2019), and identified that the temperature, surface topography, BIA, and katabatic winds enhanced the formation of SGLs. One exception to the focus on SGLs is Chen et al. (2024), who provided a snapshot of large channels (width > 30 m) on Nivlisen Ice Shelf using Landsat-8 imagery, identifying a dendritic network of 47 channels in January 2020. While they measured some fluvial metrics (e.g., channel width, depth), the temporal evolution of the SCN was not analysed.

Although these previous studies mentioned that SGLs often co-exist with supraglacial channels, they have predominantly focused on the formation, evolution and impact of the SGLs. Consequently, our understanding of SCNs, particularly their long-term meltwater routing efficiency, dynamics, and connectivity, remains limited. Furthermore, while observations suggest that these networks often spatially merge into a small number of large channels that may terminate in a large lake, it remains unclear whether this pattern is consistent across different melt seasons or occurs only sporadically. Therefore, more detailed quantification of channel networks on the Nivlisen are urgently needed to provide critical insights into the role of supraglacial channels in redistributing meltwater across Nivlisen Ice Shelf.

3 Methods

This study uses freely available satellite data to map hydrological features (including channels and lakes) across a consecutive eight-year observational period (i.e., 2017-2024) based on the availability of high-resolution imagery, and for the 2018-2019 melt season which recorded the maximum lake extent (Dirscherl et al., 2021; Arthur et al., 2022). We quantify key metrics including water area, depth, number of channels, total length of channels; and correlate them with climate variables, including temperature, snowfall, and surface melt; to identify the primary drivers influencing drainage network evolution.

https://doi.org/10.5194/egusphere-2025-5562
Preprint. Discussion started: 17 February 2026

3.1 Images and pre-processing

3.1.1 Sentinel-2

A total of 32 Sentinel-2 Level-2A (L2A) scenes (see Supplement Table 1) covering the study area were acquired between 26 January 2017 and 22 February 2024 from the Copernicus Data Space Ecosystem Browser (https://browser.dataspace.copernicus.eu last accessed: 31 July 2024) to observe the interannual variations of SCNs. Supraglacial water features were delineated using the Sentinel-2 Level-2A (L2A) images with Bottom-Of-Atmosphere reflectance values. Spectral bands at a spatial resolution of 10 m including bands 2 (Blue), 3 (Green), 4 (Red), and 8 (Near infrared, NIR) were used. Each Sentinel-2 L2A image was clipped and then mosaicked to produce temporally consistent images covering the whole Nivlisen ice shelf and reprojected to the WGS 1984 Stereographic South Pole co-ordinate system (EPSG: 3031).

3.1.2 Landsat-8

Throughout the summer of 2018-2019, the development of SCNs was monitored across eight dates dictated by cloud-free image availability. A total of 10 Landsat-8 Level-2 Surface Reflectance (SR) optical images (see supplement Table 1) spanning 8 dates were used to conduct seasonal analysis due to the limited temporal coverage of Sentinel-2 optical imagery. Full spatial coverage of the study area was achieved using mosaicked imagery for two dates (2018/12/24 and 2019/01/25), while the remaining dates were covered by a single satellite scene. The raw Landsat-8 imagery was identified and downloaded from the USGS Earth Explorer website (https://earthexplorer.usgs.gov last accessed: 31 July 2024). This part of the study specifically focussed on a single melt season from December 2018 to March 2019, because this season recorded the maximum meltwater extent and had the most cloud-free images available. Spectral bands including 1 (Blue), 2 (Green), 3 (Red), 4 (Near infrared, NIR) and 8 (Panchromatic) were used to delineate supraglacial water features. Each Landsat-8 imagery has been processed as natural-colour pan-sharpened images at 15 m spatial resolution for observing more details by using NNDiffuse Pan Sharpening Sharpening tool from ENVI 5.6 software (Harris Geospatial Solutions, 2020).

3.2 Mapping SCNs

Surface water areas were identified using the Normalised Difference Water Index for ice (*NDWIice*), which has been widely adopted to extract meltwater features on ice surfaces in polar regions (e.g., Moussavi et al., 2020; Dell et al., 2020; Tuckett et al., 2021; Yang et al., 2021; Chen et al., 2024). *NDWIice* is calculated from the normalised ratio of the blue and red bands as Eq. (1):

$$NDWI_{ice} = (Blue - Red)/(Blue + Red) \quad (1)$$

Surface water exhibits higher reflectance values in the Blue band and a relatively large contrast with the background (i.e., ice and snow) in the Red band on optical imagery (Yang and Smith, 2013). A threshold

https://doi.org/10.5194/egusphere-2025-5562
Preprint. Discussion started: 17 February 2026

of 0.20 was adopted to filter the water pixels from each *NDWIice* image, following previous studies where thresholds typically range between 0.15 and 0.30 (Stokes et al., 2019; Chen et al., 2024; Glen et al., 2025). However, we found that most water bodies detected from *NDWIice* thresholding are lakes or channels with deep water, and some thin channels which are narrower than the image resolution (approximately 10 m wide) cannot be recognised by this method (Glen et al., 2022; Langley et al., 2016). Meanwhile, some water resides in the firn and is better described as slush (Dell et al., 2020). Therefore, manual post-processing was necessary to remove some mis-classified water pixels (e.g., slush, ice background) from thresholding *NDWIice*. Uncertainties associated with this classification primarily arise from threshold selection and the delineation of water boundaries, particularly for shallow water and slush areas. Similar NDWI thresholding methods have been widely applied in previous studies of supraglacial hydrology in Greenland and Antarctica (Moussavi et al., 2020; Yang et al., 2021; Chen et al., 2024); however, robust quantification of classification uncertainty remains challenging in the absence of ground-truth observations.

Supraglacial channels and their terminus were manually identified and delineated as centrelines based on Landsat-8 and Sentinel-2 imagery. True-colour composites (Sentinel-2 bands 4-3-2, Landsat-8 bands 4-3-2) were used for visual interpretation, supplemented by the *NDWIice* image to enhance the contrast between meltwater and surrounding snow or ice. The identification relied on a combination of morphological, topographic, and contextual indicators: 1) linear geometry: water bodies exhibiting narrow, elongated shapes were considered potential channels, especially those connected with circular depressions interpreted as lakes or ponded areas; 2) topographic validation: the Reference Elevation Model of Antarctica (REMA) database (Howat et al., 2019) was used to verify whether the identified features followed a downslope path, consistent with gravitational water flow; 3) temporal consistency: where available, sequential imagery from different dates within the same melt season, which means consistently observed patterns strengthened the interpretation of channels. The delineation of surface water (i.e., vector polygon) and supraglacial channels (i.e., vector lines) are shown in Fig. 2, which was used to measure several metrics in the following analysis.

https://doi.org/10.5194/egusphere-2025-5562
Preprint. Discussion started: 17 February 2026

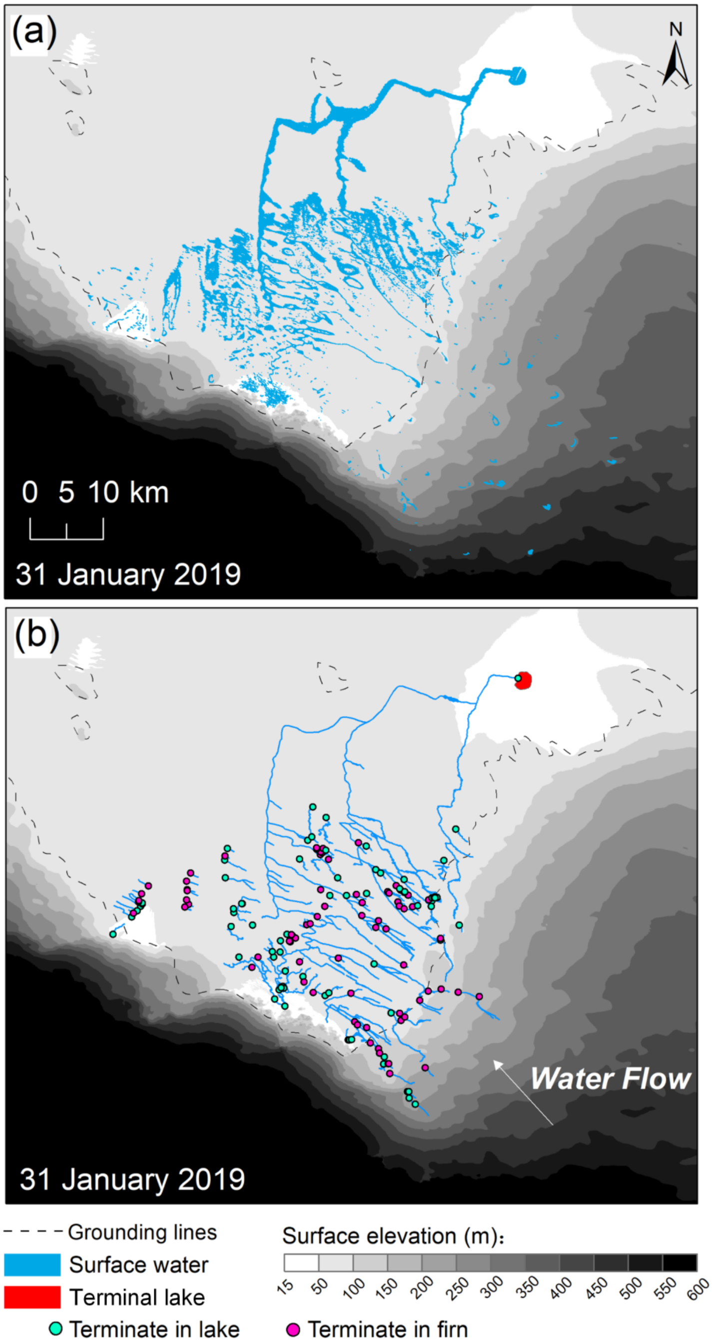

Figure 2: Supraglacial drainage systems on Nivlisen Ice Shelf on 31 January 2019: (a) detected surface water using the *NDWIice* and (b) centrelines of manually mapped channels and channel termini (see Section 3.3). The base image is the REMA 10 m DEM data (Howat et al., 2019).

https://doi.org/10.5194/egusphere-2025-5562
Preprint. Discussion started: 17 February 2026

3.3 Quantifying the morphometry of SCNs

3.3.1 Key metrics of SCNs

Based on the digitized water polygons and channel centrelines (e.g. Fig. 2b), several key metrics (surface water area, water depth, number of channels, total channel length and number of SCNs) (Table 1) were measured using tools from ArcMap 10.8 (Yang et al., 2016). In addition, we used the mosaiced surface elevation model (DEM) data at 10 m spatial resolution from the REMA database (Howat et al., 2019) to approximate surface water elevation by ArcMap 10.8. Channel Density, defined as the total length of supraglacial channels per unit area (m km^{-2}), characterizes the spatial concentration of meltwater channels. The ice shelf surface was divided into 5 km ×5 km grid cells using the Fishnet tool in ArcGIS Pro 2.8.8, allowing spatially consistent drainage density calculations across different timescales. To assess whether there are statistical differences between time periods, non-parametric Kruskal–Wallis H-tests (Ostertagová et al., 2014) were conducted independently for depth and elevation.

Table 1. Summary of measured metrics

Metric	Unit	Indicates	Description
Water area	m^2	Surface melt extent	total area covered by visible water bodies from satellite imagery, including channels and lakes
Elevation	m	Surface drainage distribution	surface elevation of visible channels networks from REMA DEM image, excluding lakes
Depth	m	Meltwater volume	depth from surface to bottom of the water in channels networks, excluding lakes
Channel length	m	Flow path development	the path distance between segment endpoints
Number of channels	n	Drainage complexity	total count of visually identified linear channels
Number of channel networks	n	Connectivity/network integration	count of independent connected components
Channel density	m km^{-2}	Drainage efficiency	total channel length divided by surface area grids

To identify which channels are connected to each other, the mapped vector centrelines were converted into binary (water and ice background) images with the spatial resolution of satellite imagery (Sentinel-2: 10 m, Landsat-8: 15 m). Channel pixels that meet the adjacency criterion for 8-neighbor connectivity (i.e., share an edge or a vertex) (He et al., 2017) are recognised as being members of the same channel network (Fig. 3). The binary image was then converted back into vector polylines, where polylines

https://doi.org/10.5194/egusphere-2025-5562
Preprint. Discussion started: 17 February 2026

belonging to the same network are marked with the same component ID, indicating they are channels within the same network.

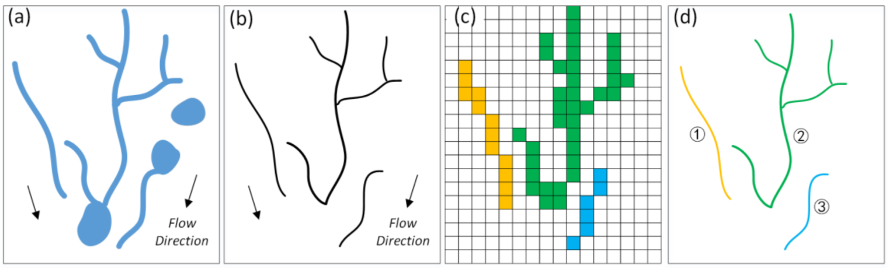

Figure 3: Schematic of supraglacial channel network detection: (a) original supraglacial water features mapped from satellite imagery, (b) vector centrelines of SCNs, (c) binarized raster of vector centrelines and (d) identified connected channels using 8-neighbors pixel connectivity.

3.3.2 Estimation of surface water depth

To assess interannual variability in surface water depth from Sentinel-2 imagery, we applied a satellite-derived depth retrieval algorithm based on reflectance-depth relationships which is widely used over the Greenland and Antarctic ice sheets (Williamson et al., 2018; Zhang et al., 2023; Melling et al., 2024). This empirical power-law formulation (d_{pixel}, in m) is:

$$d_{pixel} = 0.2764 \times Red^{-0.8952} \tag{2}$$

where *Red* represents the reflectance value of the Sentinel-2 Red band. For Landsat-8 imagery, a spectral band ratio approach has been adopted to derive water depth based on the dual-channel model (Eq. 3-4) (Moussavi et al., 2016; Pope et al., 2016). The empirical derivation of calibrated coefficients is (Pope et al., 2016):

$$z = a + bX + cX^2 \tag{3}$$

$$X = \ln(Band_1/Band_3) \tag{4}$$

where $a = 0.1488$, $b = 5.0370$ and $c = 5.0473$, $Band_1/Band_3$ is the ratio of the reflectance values of Landsat-8 OLI Band-1 (Coastal/Aerosol: 0.435-0.451 μm) and Band-3 (Green: 0.533-0.590 μm), and z stands for the derived water depth from Landsat-8 imagery.

While subject to large uncertainties in absolute depth estimation due to the lack of in situ validation, this result provides a consistent relative metric for tracking year-to-year hydrological changes and allows a first order estimate of water depths. The derived depth images have been masked with the thresholded *NDWIce* water outlines to obtain the results.

https://doi.org/10.5194/egusphere-2025-5562
Preprint. Discussion started: 17 February 2026

3.4 Comparison with climatic variables

Climate variables including snowfall, surface melt and air temperature have been identified as key controls on surface melt and the ponding of surface water in Antarctica (Langley et al., 2016; Kittel et al., 2021; Arthur et al., 2022). To identify potential meteorological controls on SCN variability, we conducted correlation analyses between four hydrological parameters and seven climate variables spanning multiple temporal scales. The four hydrological parameters are: (1) surface water area, (2) mean water depth, (3) SCN count, and (4) channel density. The first five climate variables are from the Modèle Atmosphérique Régionale (MAR) regional climate model (MARv3.11) (Kittel et al., 2021): (1) austral winter snowfall (June to August accumulation), (2) austral spring snowfall (September to November accumulation), (3) austral summer snowfall (November to January accumulation), (4) summer season melt (November to January accumulation), and (5) austral summer surface mass balance (November to January net accumulation). The final two climate variables are: (6) near-surface 2 m air temperature (T_{2m}) at 0.1° resolution from the European Centre of Medium-range Weather Forecasts Reanalysis v.5 (ERA5) global reanalysis (Hersbach et al., 2020) and (7) local temperature data from Novolazarevskaya Research Station (70°46′S 11°52′E, Fig.1b) *in-situ* records acquired by the REference Antarctic Data for Environmental Research (READER) Project (Turner et al., 2004). Daily MAR outputs (mm w.e. day^{-1}) were summed over the corresponding seasons to obtain accumulated melt, snowfall, and SMB values (mm w.e.). Climate variables were primarily chosen from the MAR climate model because it provides physically consistent surface mass balance components for ice sheets and ice shelves at a high spatial resolution. Meanwhile, the 2 m air temperature data were obtained from ERA5 because it is a well-validated, observation-constrained variable and is widely used as an independent benchmark for representing surface melt conditions (Arthur et al., 2022). MAR outputs represent deterministic model results for each year, and associated uncertainties are not explicitly quantified but are typically evaluated through interannual variability, sensitivity to model forcing, and comparison with independent datasets. Pearson correlation analyses were performed between all combinations of one of the four hydrological metrics and one of the seven climate variables (Zhang et al., 2023).

For seasonal analysis, the cumulative values of several climate variables (i.e., melt, 2 m air temperature, SMB-surface mass balance and snowfall) were calculated over fixed time windows preceding each channel network observation date (i.e., 7-day and 14-day) (Dirscherl et al., 2021), which allows us to explore lagged cumulative forcing analysis of climate variability on evolution of SCNs. Specifically, only values exceeding melt-relevant thresholds were retained for some variables (e.g., maximum air temperature > 0 °C for Positive Degree Days (PDD)), while others were directly accumulated without thresholding. The resulting cumulative indicators were then correlated with measured metrics (e.g., water area, total channel length) using Pearson correlation.

https://doi.org/10.5194/egusphere-2025-5562
Preprint. Discussion started: 17 February 2026

4 Results

4.1 Interannual evolution of SCNs

4.1.1 Interannual spatial distribution of SCNs

The Nivlisen Ice Shelf exhibited strong interannual variability in the extent and structure of SCNs from 2017 to 2024 (Fig. 4). A total of 710 SCNs comprising 5513 individual channels were mapped, with approximately 52 % terminating in lakes and 48 % draining into the firn layer, i.e. with no obvious lake at the terminus. The SCNs expanded markedly between 2017 and 2018, reaching a peak in 2018 in terms of surface water area. In 2019 and 2020 the three main channels (marked as West (WS), Middle (M) and East (ES)) connected to form the largest observed network and terminated in a large (2019: 4.3 km^2, 2020: 10.1 km^2) lake (see Section 4.1.3, Fig. 8). From 2021 onwards, the channel networks were not as well developed. Surface water area fell to 46 km² in 2021, and no visible surface water was detected in January 2022. In 2023 and 2024, surface water partially reappeared, but the metrics remained lower than pre-2021 levels (Fig.4g-h). Spatially, the southern-most region of the grounding line consistently hosted recurring SCNs throughout all years, whereas other regions displayed high interannual variability.

https://doi.org/10.5194/egusphere-2025-5562
Preprint. Discussion started: 17 February 2026

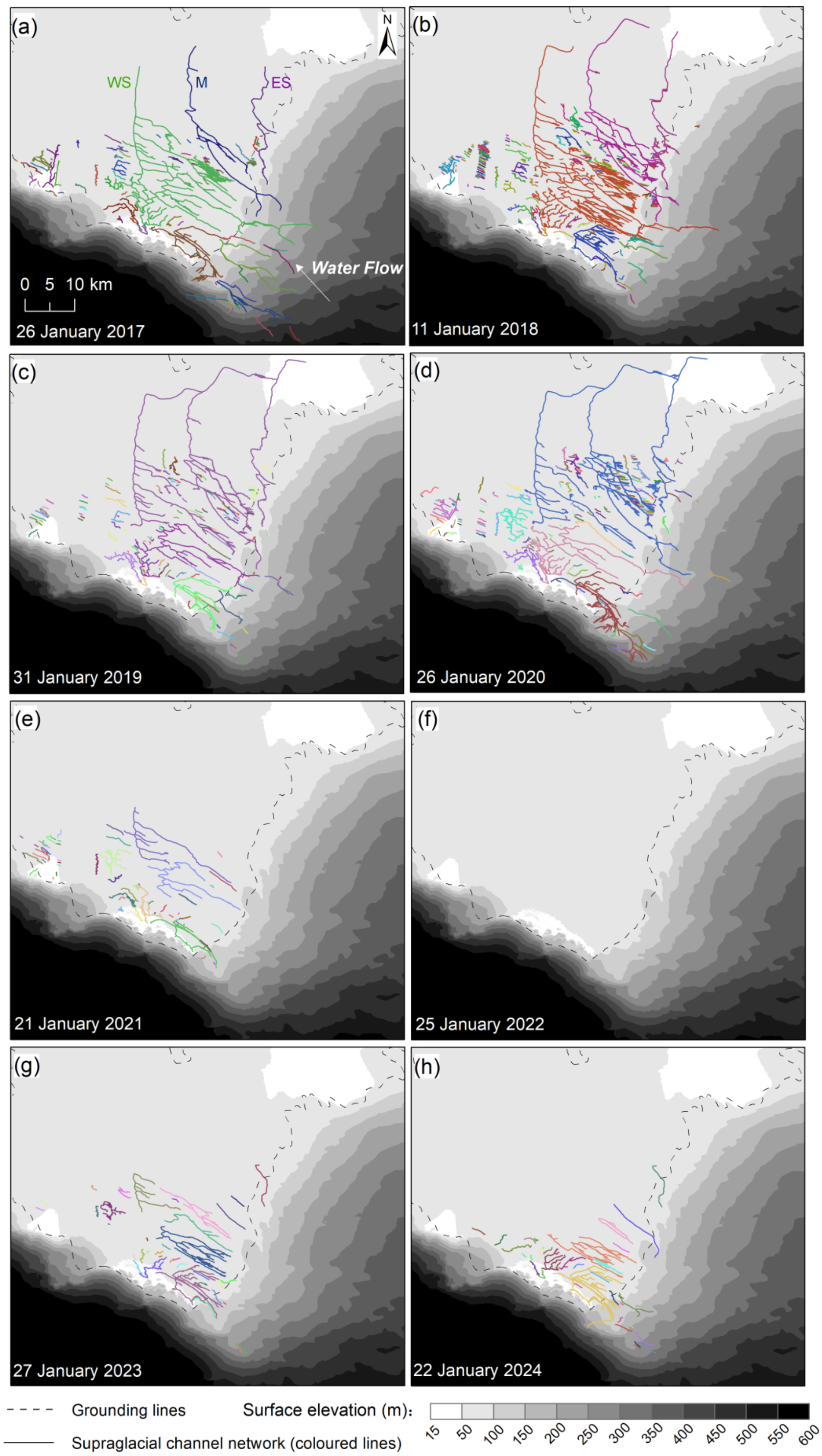

334

https://doi.org/10.5194/egusphere-2025-5562
Preprint. Discussion started: 17 February 2026

Figure 4: Interannual evolution of SCNs on Nivlisen Ice Shelf from 2017 to 2024. The solid lines in different colours represent separate SCNs in each year. The base image is REMA DEM data at 10 m resolution (Howat et al., 2019). Three main channels marked as West (WS), Middle (M) and East (ES) are shown in (a).

Figure 5 illustrates the interannual variability of surface water area, number of channels, total channel length, and number of channel networks over the eight-year study period. All metrics reach a peak in 2018, when the surface water area was approximately 172 km^2. In 2018, there were 186 channel networks, 1650 channels, and the total channel length exceeded 1400 km, indicating a widespread and well-connected drainage network. However, while the surface water area decreased from ~140 km^2 in 2019 to ~135 km^2 in 2020, the number of channels increased from 938 to 1373, and total channel length increased from 895 km to 1275 km. In 2022 there was a sharp decline of all metrics to zero. Partial recovery is observed in 2023 and 2024, but the surface water area remained below 50 km^2, and channel-related metrics did not return to pre-2022 levels (e.g., 319 channels and 419 km of total length in 2023).

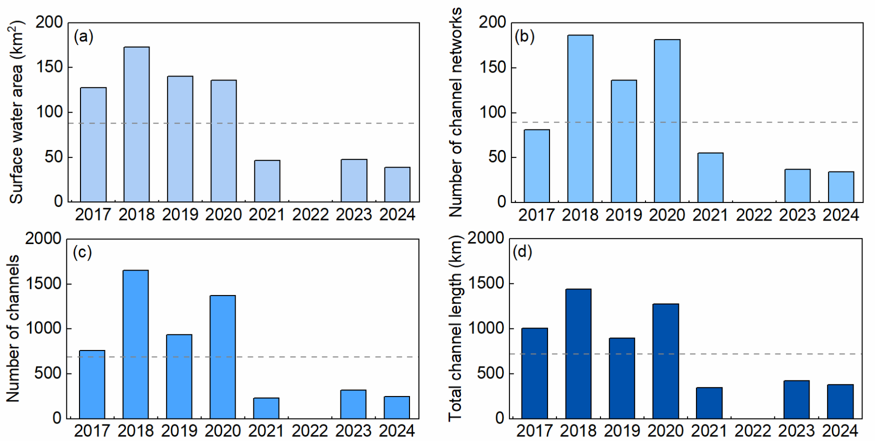

Figure 5: Interannual variations in total water area, number of channels, total length of channels and number of SCNs on Nivlisen Ice Shelf. Values represent annual total metrics derived from a single observation for each melt season. The grey dashed lines represent the mean value of each metric.

Kruskal-Wallis tests reveal statistically significant interannual differences in both surface water elevation and depth. For elevation, the test yielded H = 5005.60 ($p < 0.001$), although the high significance likely reflects the large sample size rather than a substantial shift in distribution. The median elevations remained broadly consistent during the study period, with most SCNs concentrated around 70 m a.s.l. (Fig. 6). A slight decrease occurred only in 2021, when the mean elevation was lower and the minimum approached 60 m. For depth, the Kruskal-Wallis test also returned a significant result (H = 17179.2, $p < 0.001$). Median depths were about 0.4 m from 2017 to 2021, and decreased slightly to ~ 0.3 m in 2023

https://doi.org/10.5194/egusphere-2025-5562
Preprint. Discussion started: 17 February 2026

and 2024. Despite the statistical significance, these results indicate that both elevation and depth remained relatively stable through most of the study period.

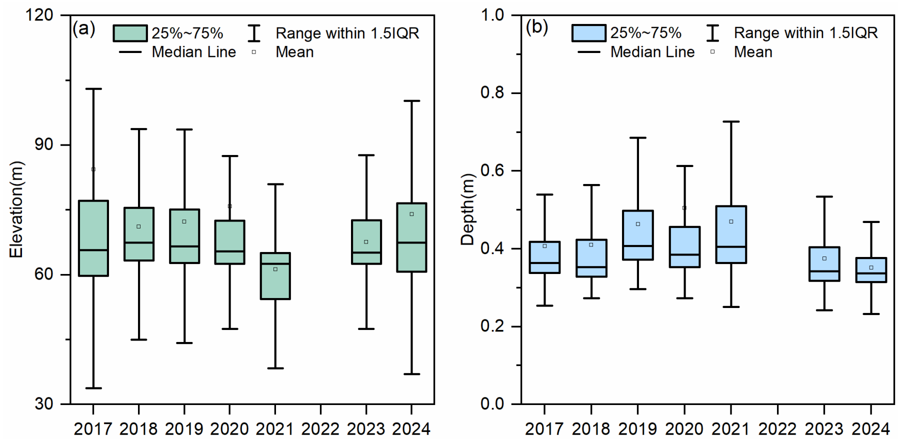

Figure 6: Interannual variation in the (a) elevation and (b) water depth of SCNs on Nivlisen Ice Shelf from 2017 to 2024. Medians and interquartile ranges are shown. Kruskal-Wallis tests confirm significant interannual variability for both variables ($p < 0.001$).

4.1.2 Interannual variations in channel density and channel reoccurrence

The interannual variability in drainage density, with high drainage density (> 2200 m of cumulative channel length per km^2) represented by dark blue colours in Fig. 7. From 2017 to 2018, the highest density regions are in the eastern parts of the ice shelf, close to the grounding line. Although the spatial footprint of SCNs extends slightly northward in 2019, the overall drainage density decreases compared to 2018, as indicated by the reduction in dark blue grid cells (> 2400 m km^{-2}). This shift coincides with a reduction in the number of channel networks, suggesting that meltwater pathways became more spatially fragmented. In 2020 there is an appearance of more high-density areas, which shift towards the southern and northern regions, showing the formation of new channels. 2021 likely marks a transition year, where surface melt was greatly suppressed, and channel networks disintegrated into sparse, fragmented parts with limited connectivity or meltwater supply. From 2021 to 2024, with the exception of 2022, few regions covered by SCNs exceeded 1000 m km^{-2}. Overall, the high-density regions exhibit significant spatial and temporal shifts during the study period. The reoccurrence map in Fig. 7(h) reveals that over the eight years, SCNs frequently appeared in the areas near the southernmost part of grounding line, particularly near the Schirmacher Oasis nunatak (i.e., dark red grids near the grounding line). These high reoccurrence zones represent long-lived hydrological pathways, where supraglacial channels are usually active across multiple years, despite interannual variability in meltwater supply.

https://doi.org/10.5194/egusphere-2025-5562
Preprint. Discussion started: 17 February 2026

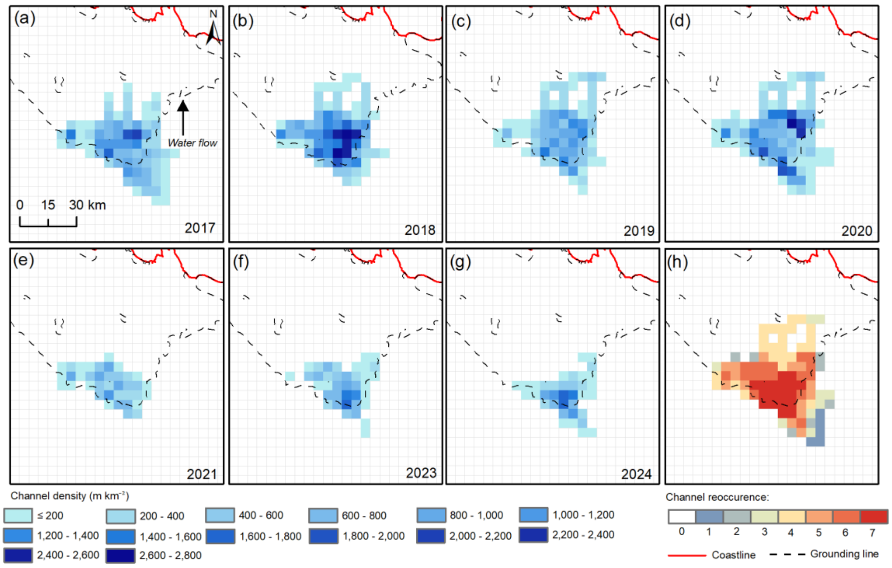

Figure 7: Interannual channel density (a)-(g) and channel reoccurrence (h) of the SCNs on Nivlisen Ice Shelf from 2017 to 2024. Note that no channels developed in 2022 (see Fig. 4-5).

4.1.3 Reoccurrence of the large terminal lake in 2019 and 2020

A large supraglacial lake formed at the confluence of the WS, M, and ES channels during the summers of 2019 and 2020 (Fig. 8). On 31 January 2019, the lake was a dark-blue colour and covered an area of 4.35 km² (Fig. 8a). By 26 January 2020, the same ice surface depression contained a larger lake of 10.1 km² in area, but the water appeared shallower, as indicated by its lighter tone (Fig. 8b). Sentinel-2 imagery from 2020 also reveals a distinct ~50 m-wide frozen rim extending beyond the visible water margin, a feature absent in January 2019, suggesting gradual refreezing during late summer. These contrasting observations indicate that the lake experienced markedly different storage capacities and drainage regimes between the two years but that there is also a challenge in understanding its evolution in scale due to the pattern of refreezing and subsequent re-melting.

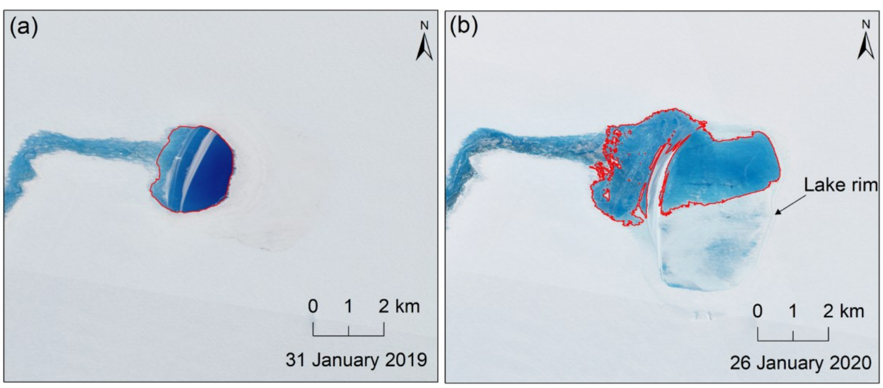

Figure 8: Comparison of supraglacial lake evolution on Nivlisen Ice Shelf between 2019 and 2020: (a-b) Sentinel-2 images on 31 January 2019 and 26 January 2020, respectively, with lake boundaries shown in red. In 2020, a prominent peripheral rim is visible around the enlarged lake. In 2019, the lake was smaller (4.35 km^2) but substantially deeper (up to ~8 m). By contrast, in 2020 the lake expanded to 10.1 km^2 but was considerably shallower (< 2 m), with the outer rim extending ~50 m beyond the visible water surface.

4.2 Seasonal evolution of SCNs

4.2.1 Seasonal spatial distribution of SCNs during a melt season

Throughout the 2018-2019 melt season, the SCNs evolved from fewer and disconnected water bodies to complex, integrated systems and eventually returned to more fragmented networks (Fig. 9). In early December (1 and 10), sparse and isolated water bodies were distributed across the ice shelf. As the season progressed into mid- to late- December, supraglacial channelisation became increasingly pronounced, particularly near the grounding line, with numerous short and fragmented channels with limited connectivity. Meanwhile, SGLs at high elevations decreased in size and, in some cases, disappeared completely by 24 December. By late January, SCNs reached their maximum spatial extent, characterized by extensive branching and well-developed main channels spanning broad regions of the ice shelf. This phase exhibited higher degrees of interconnection between individual SCNs, suggesting the integration of previously independent networks. Notably, those SGLs that had previously vanished in high-elevation regions reappeared with reduced surface areas. In February and early March, the SCNs began to fragment, with fewer continuous structures and reduced extent. Despite this decline, some main channels remained well-defined until early March, particularly in lower-elevation areas (Fig. 9f-h).

https://doi.org/10.5194/egusphere-2025-5562
Preprint. Discussion started: 17 February 2026

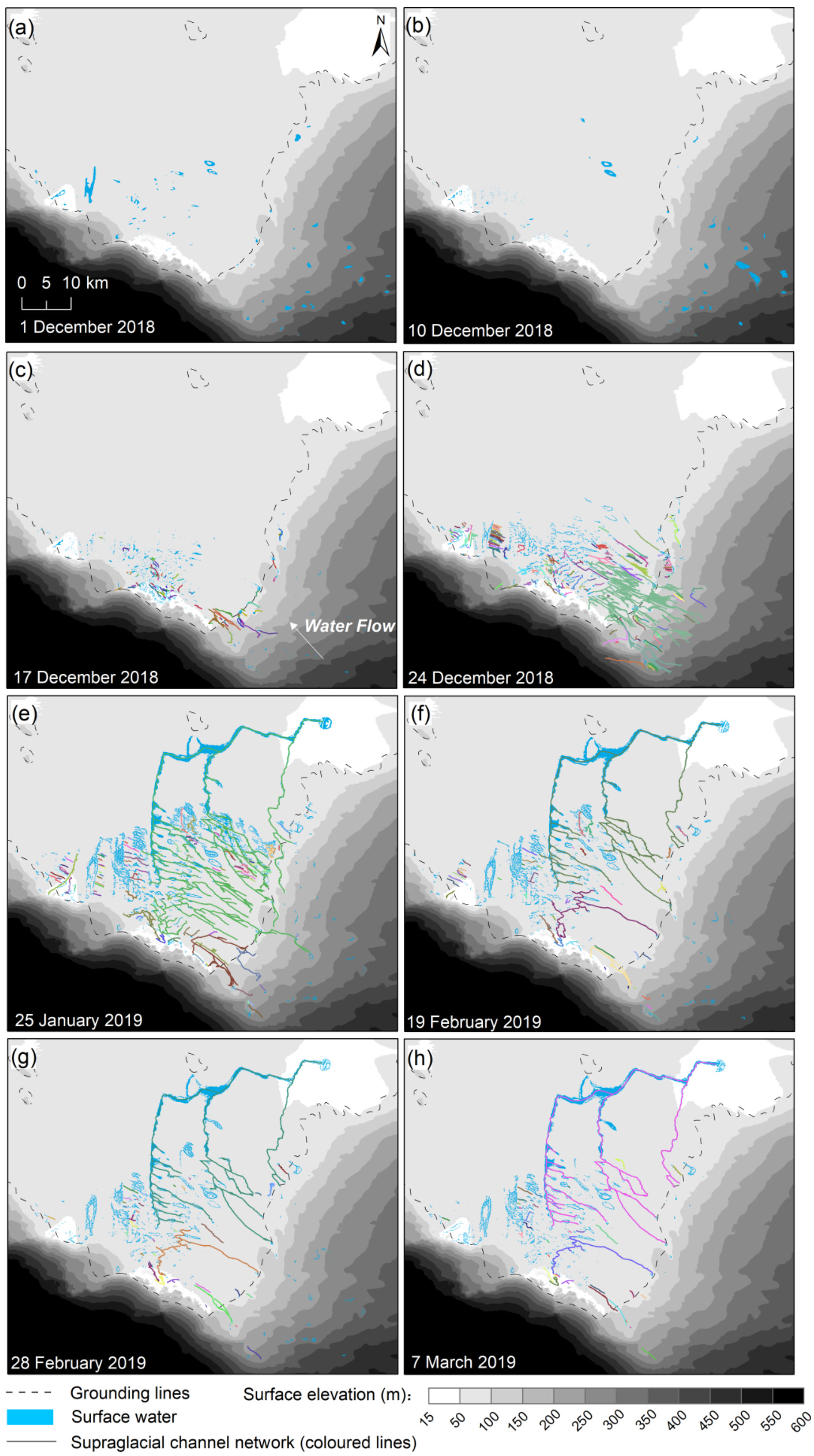

https://doi.org/10.5194/egusphere-2025-5562
Preprint. Discussion started: 17 February 2026

Figure 9: Seasonal evolution of SCNs on Nivlisen Ice Shelf in melt season from 2018 December to 2019 March. The solid lines in different colours represent separate SCNs delineated manually, and the blue polygons indicate the automatically mapped surface water during the melt season. The base image is REMA DEM data at 10 m resolution (Howat et al., 2019).

Quantitative metrics clearly show the seasonal evolution of SCNs on Nivlisen Ice Shelf (Fig. 10). By 25 January 2019, surface water area peaked at approximately 191 km², accompanied by the development of 924 individual channels with a total length of 967 km. This peak reflects the most widespread drainage of the melt season. Interestingly, despite the expansion in the number and extent of channels, the number of individual SCNs decreased after 24 December (from ~170 to ~100), suggesting enhanced connectivity. Following this peak, all metrics steadily declined into February and March. By 7 March, surface water area had dropped to ~83 km², with fewer than 300 channels remaining and the total channel length reduced to below 35 km.

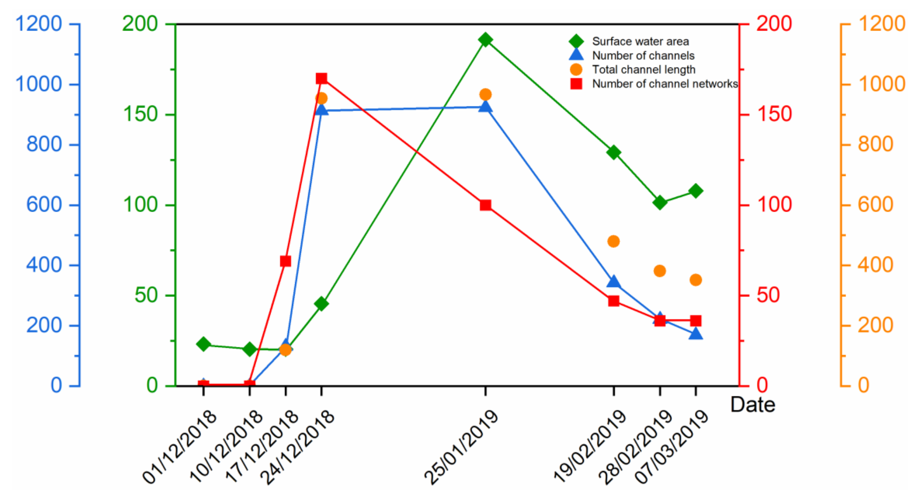

Figure 10: Seasonal variations in total water area, number of channels, total length of channels and number of SCNs on Nivlisen Ice Shelf.

Both observations from satellite images (Fig. 9) and Kruskal-Wallis test indicate significant seasonal variation in the elevation of SCN development ($H = 5310.2$, $p < 0.001$). Starting from 17 December, when channels were first observed, the elevation range widened slightly during early melt and then gradually narrowed. By late January, most SCNs were restricted to lower-elevation areas below 100 m a.s.l., where the values remain stable throughout February and March. This pattern indicates a downslope migration of surface meltwater over the melt season, consistent with surface drainage toward the grounding line and ice shelf front (Fig. 9). For depth, the Kruskal-Wallis test showed a significant result ($H = 7490.4$, $p < 0.001$), although visual inspection suggests that the magnitude of variation was limited. The depth of SCNs on Nivlisen Ice Shelf generally increased from late December, peaked in late January,

https://doi.org/10.5194/egusphere-2025-5562
Preprint. Discussion started: 17 February 2026

and then declined toward early March during the 2018-2019 melt season (Fig. 11a). In the early season (1-10 December 2018), water in SCNs was shallow (mostly less than 1 m) and exhibited low variability. Mean water depth increased notably from late December 2018, reaching a maximum on 25 January 2019, when the mean values were greater than 0.8 m. From 19 February to 7 March, mean water depth steadily decreased and became more uniform, suggesting refreezing and a reduction in meltwater supply toward the end of the melt season.

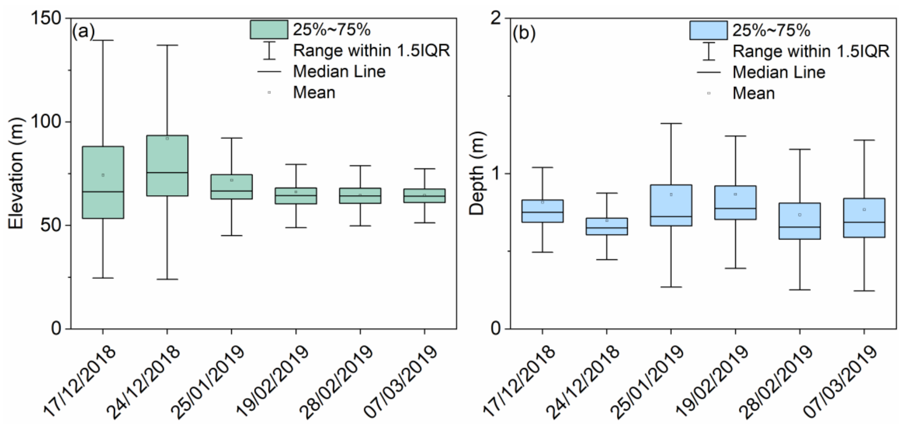

Figure 11: Seasonal variation in the (a) elevation and (b) water depth of SCNs on Nivlisen Ice Shelf during the 2018-2019 melt season. Kruskal-Wallis tests confirm significant seasonal variability for both variables ($p < 0.001$).

4.2.2 Seasonal evolution of channel density and connectivity

Gridded channel density maps (Fig. 12) reveal a clear seasonal progression in the spatial extent and density of supraglacial channels on Nivlisen Ice Shelf during the 2018-2019 melt season. Initially sparse and localized in mid-December (mostly less than 600 m km^{-2}), channel density peaked in magnitude in late December (with values exceeding 2,800 m km^{-2} in some grid cells near the grounding line). By January, drainage pathways became fully established, with channels extending across nearly the entire ice shelf surface. The densest networks formed continuous connections between the grounding zone and the ice-shelf front, reflecting a phase of maximum hydrological connectivity and widespread surface meltwater transport. Thereafter, channel density declined steadily into February and March which was less than 400 m km^{-2}.

https://doi.org/10.5194/egusphere-2025-5562
Preprint. Discussion started: 17 February 2026

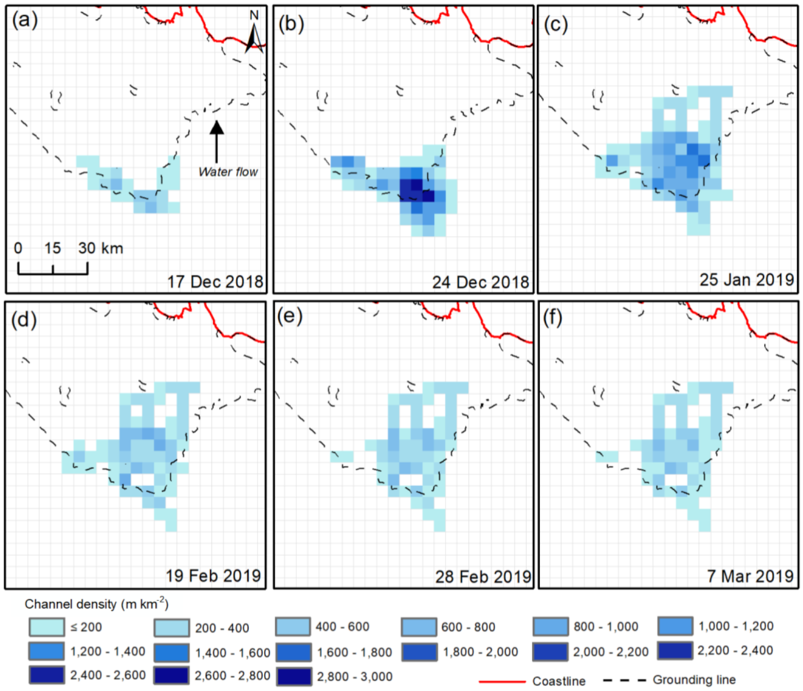

Figure 12: Seasonal channel density of the SCNs on Nivlisen Ice Shelf during the meal season in 2018-2019.

To illustrate how supraglacial connectivity evolves during the melt season in 2018-2019, overlapping channel networks across six key dates are shown in Fig. 13a. These patterns reveal a clear trend towards increased connectivity and a progressive downslope transportation of meltwater, originating from high-elevation areas in the southeast above the grounding line and extending across the grounding line toward the ice edge. Throughout this period, active channels either persisted, disappeared, or merged into more integrated networks, reflecting dynamic reorganisation of surface drainage pathways. Upon examining the SCNs across the entire study area during the melt season, two representative zones were selected to illustrate the impact of local topography on the spatial evolution of SCNs (Fig. 13b-i). Zone 1 is characterized by a significant elevation transition, and Zone 2 is a relatively flat area. On 17 December 2018, both zones exhibited fragmented and dispersed channel networks, indicating an early stage of isolated channel development with limited interconnectivity. After seven days (24 December 2018), some of the channels in Zone 1 disappeared (grey lines in Fig. 10c), while others merge into larger and more integrated networks, allowing surface water to traverse the grounding line along the northwest direction. In contrast, Zone 2 experienced an increase in channel formation (both quantity and total length) during this interval, with newly created SCNs developing in a more focused southward flow pattern. On 25 January 2019, the SCNs in Zone 1 exhibited further transformation, as many previously active channels disappeared, and the remaining networks were more widely spaced. However, during the same period in Zone 2, a number of channels joined and formed more integrated networks. In the late summer

https://doi.org/10.5194/egusphere-2025-5562
Preprint. Discussion started: 17 February 2026

(19 February 2019), more than 70 % of the SCNs in both zones had become invisible from the Landsat-8 imagery, which is likely associated with reduced meltwater supply and seasonal shutdown of surface drainage.

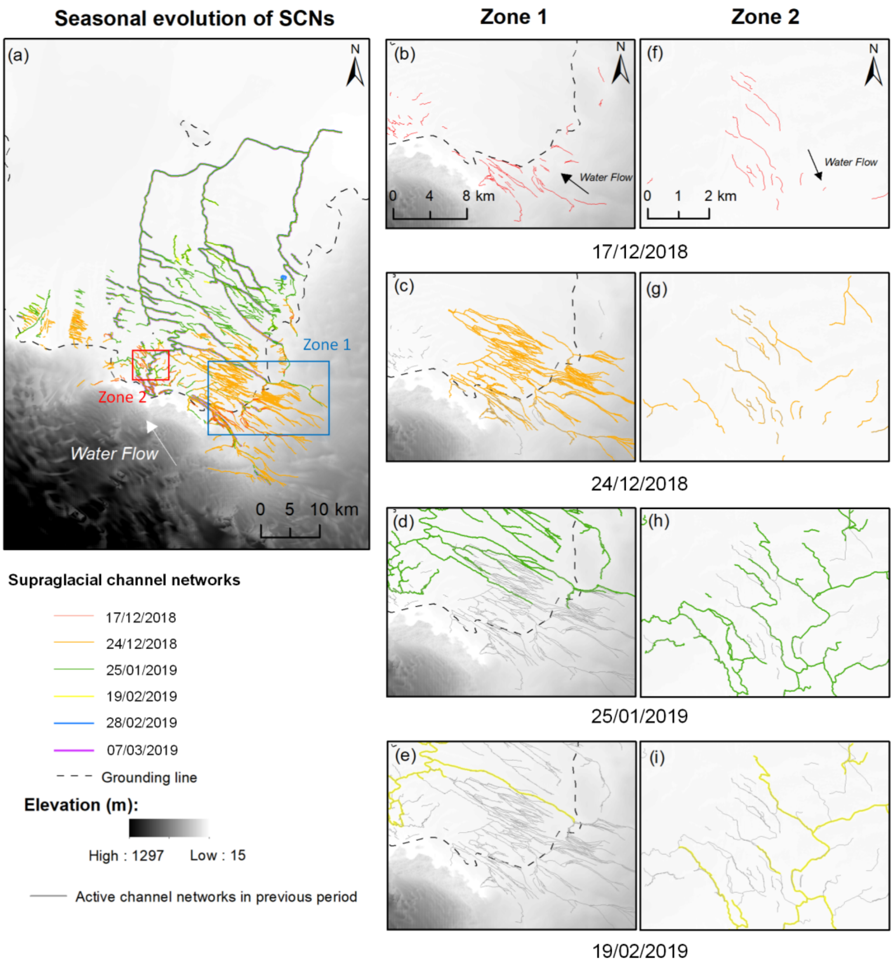

Figure 13: Seasonal connectivity transition of the SCNs on Nivlisen Ice Shelf in summer of 2018-2019. The solid lines represent the SCNs in sequential time periods. The based image is REMA DEM image at 10 m spatial resolution (Howat et al., 2019).

4.3 Controls on development of SCNs

4.3.1 Ice surface topography and channel development

Supraglacial channels on Nivlisen Ice Shelf generally followed the direction of ice surface 'flow-stripes' (Glasser and Gudmundsson, 2012a), particularly the narrower tributaries. During January 2019 and

https://doi.org/10.5194/egusphere-2025-5562
Preprint. Discussion started: 17 February 2026

January 2020, the three main channels (i.e., WS, M, and ES) connected with each other to form the most extensive drainage network observed (Fig. 4c-d). Notably, the main channel exhibits an abruptly sharp ~90° eastward turn after merging. To understand this behaviour, we extracted surface elevation profiles along the WS channel and a nearby reference line crossing the turning point of channel (Fig. 14). The results reveal a distinct local surface high coincident with the deflection, suggesting that topography forces meltwater to reroute around this rise. The same diversion was observed in summers of 2018, 2019 and 2020, confirming that this feature represents a stable, topographically controlled pathway. Downstream of the turning point, the channel terminates in a large supraglacial lake, visible in the summers of 2019 and 2020 (Section 4.1.3).

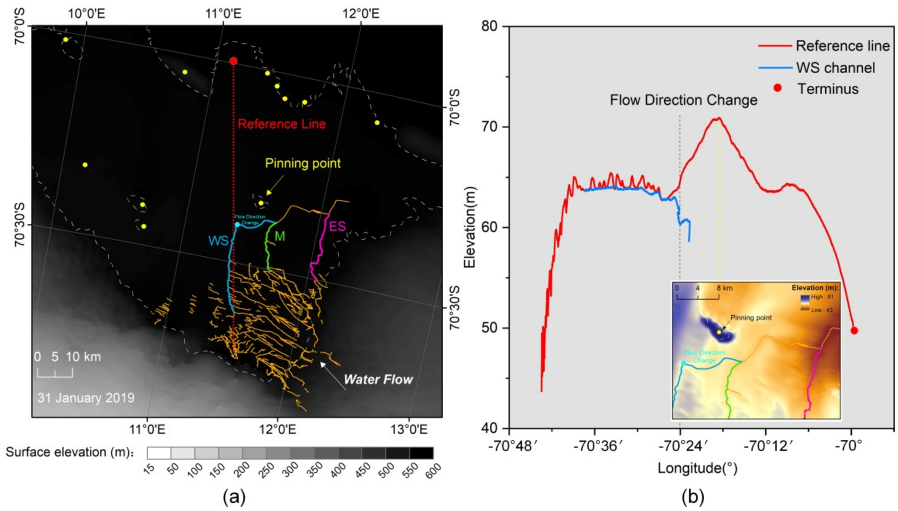

Figure 14: (a) Surface elevation map of the ice shelf on 31 January 2019, showing the locations of major channels (WS, M, ES), their confluence, and the flow direction after merging. The yellow dots represent pinning points data from Miles and Bingham (2023). The pinning point near the WS channel leads to a localised ice rumple that diverts the main channel. (b) Elevation profiles along the WS channel (blue) and a reference line on the ice shelf surface (red). The subplot in Fig. 13b shows a zoom-out elevation map near the pinning point. A notable surface high along the reference profile corresponds with a sharp flow direction change in the WS channel, suggesting topographic control of meltwater routing.

4.3.2 Climatic influences on development of SCNs

Climatic variables have been extracted from the MAR climate model outputs, including the melt, SMB and snowfall, reveal pronounced variability across the study period (Fig. 15). Summer melt experienced a sharp reduction between 2017 and 2018, followed by a gradual increase until 2023, whereas summer SMB remained relatively consistent. Seasonal snowfall fluctuated considerably (Fig. 15b), with exceptionally high summer snowfall in 2022 occurring mainly before the Sentinel-2 imagery we acquired

https://doi.org/10.5194/egusphere-2025-5562
Preprint. Discussion started: 17 February 2026

on 22 January 2022, thereby obscuring meltwater features and contributing to the apparent absence of surface water in the optical record. Mean summer air temperature (MST) comparisons between ERA5 reanalysis and research-station records (Fig. 15c) indicate similar interannual patterns but systematically higher station-based values, attributable to differences in spatial representativeness between point and modelled data. Importantly, summer melt does not directly enter the SMB budget as a negative term. Only runoff contributes to mass loss in MAR, while a substantial fraction of meltwater refreezes within the firn layer. As a result, years with high melt and moderate snowfall (e.g., 2017) can still exhibit near-zero summer SMB.

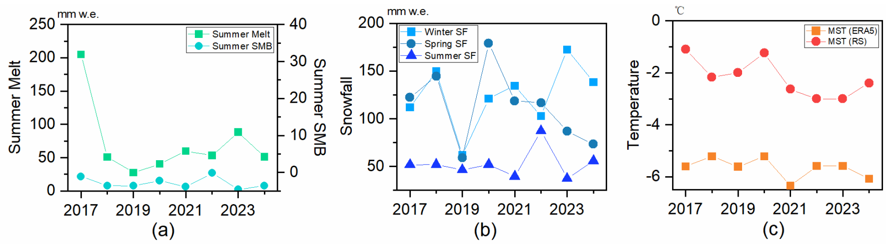

Figure 15: Interannual variations in key climatic variables over Nivlisen Ice Shelf from 2017 to 2024: (a) summer melt and summer SMB, shown as accumulated values over November-January, derived from MAR model outputs, (b) seasonal snowfall (winter, spring, and summer) from MAR, shown as accumulated totals over austral winter (June-August), spring (September-November), and summer (November-January) , and (c) mean summer temperature (MST) derived from ERA5 reanalysis and *in-situ* Research Station (RS) records.

To quantitatively assess the relationships between climatic conditions and supraglacial drainage characteristics, Pearson correlation coefficients were calculated between climatic factors (spring/summer/winter snowfall, summer melt/temperature/SMB, PDD) and characteristics of the SCNs (Fig. 16). All four metrics of the SCNs are highly correlated with each other, suggesting a coherent evolution of supraglacial drainage networks on Nivlisen Ice Shelf. MST data from ERA5 shows a statistically strong and significant positive correlation with all four metrics of the SCNs ($r > 0.9$, $p < 0.05$). Notably, mean summer temperature exerts the strongest control on total channel length ($r = 0.99$) and number of channels ($r = 0.97$). However, *in-situ* MST data from the Novolazarevskaya Research Station exhibits weaker positive and non-significant correlations ($p > 0.05$) with all SCN-related metrics. Summer SMB has positive relationships with surface water area ($r = 0.48$) and the SCNs ($r = 0.35$ and $r = 0.52$), though none are significant.

https://doi.org/10.5194/egusphere-2025-5562
Preprint. Discussion started: 17 February 2026

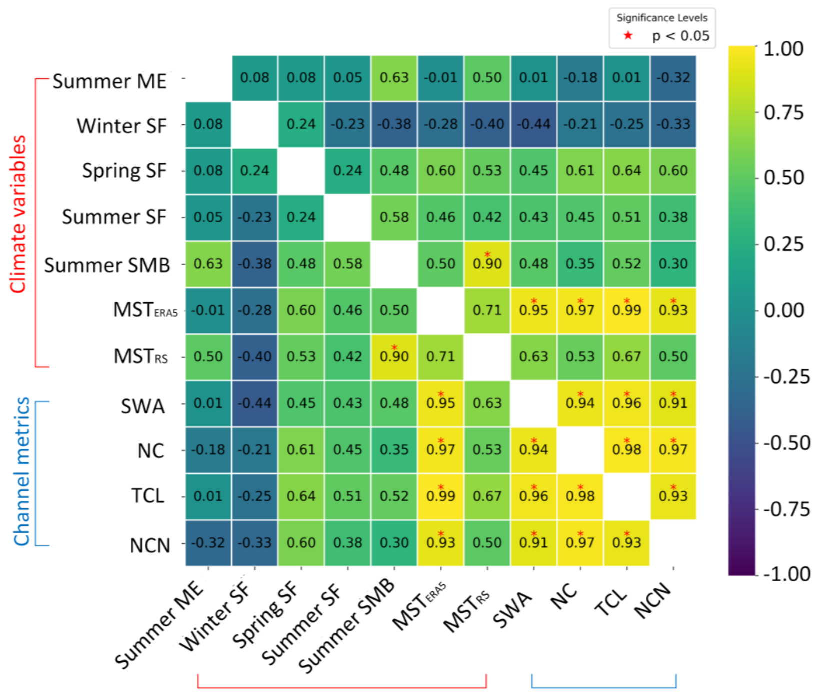

Figure 16: Linear relationships between climatic variables from MAR, ERA5 and interannual key metrics of SCNs on Nivlisen Ice Shelf. Black numbers indicate the Pearson correlation coefficient. Climatic variables: ME-melt; SF-snowfall; SMB-surface mass balance; MST-mean summer temperature. SCN metrics: SWA-surface water area; NC-number of channels; TCL-total channel length; NCN-number of channel networks.

The short-term variations in key climatic variables during the 2018-2019 melt season on Nivlisen Ice Shelf are shown in Fig. 17. Melt and SMB exhibited pronounced fluctuations throughout the season (Fig. 17a-b). The melt increases rapidly in late December, reaching its peak in mid-January, and subsequently declines toward early March. SMB generally follows an inverse pattern, becoming most negative when melt peaks, reflecting enhanced surface ablation. Snowfall shows strong temporal variability (Fig. 17c), with two pronounced events in mid-December and late February that likely influenced surface albedo and temporarily suppressed melt. Positive Degree Days (PDD) from ERA5 reanalysis over both 7-day and 14-day windows (Fig. 9d) closely track the temporal evolution of melt, confirming that short-term temperature fluctuations exert a strong control on melt intensity.

https://doi.org/10.5194/egusphere-2025-5562
Preprint. Discussion started: 17 February 2026

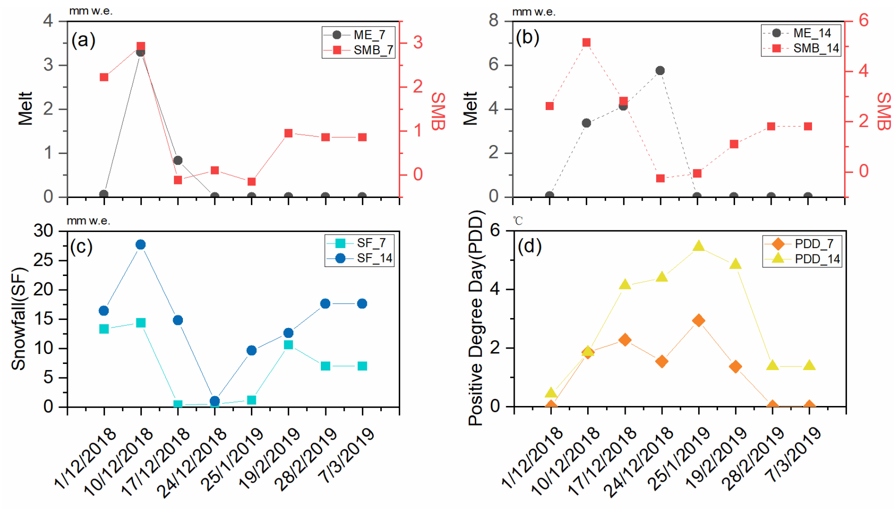

Figure 17: Short-term variations of climatic variables over the Nivlisen Ice Shelf during the 2018–2019 melt season. (a-b) Melt (ME) and surface mass balance (SMB), (c) snowfall (SF), and (d) Positive Degree Days (PDD) from ERA5 reanalysis. Variables computed over 7-day and 14-day windows are indicated by subscripts '_7' and '_14'.

On a seasonal scale, both 7-day and 14-day cumulative climate variables from ERA5 and MAR climate model influence SCN evolution (Fig. 18), with 14-day surface melt (ME_14) having the strongest and most significant correlation with number of channels ($r = 0.81$) and number of SCNs ($r = 0.80$). The correlation between PDD_14 and total channel length ($r = 0.73$, $p < 0.05$) further confirms the sensitivity of SCN spatial expansion to short-term cumulative melt. Snowfall and SMB were negatively correlated with SCN formation, and in particular, snowfall with 14-day accumulation (SF_14) is significantly negatively correlated with surface water area, implying that the snowpack inhibited or masked meltwater pooling and channels formation. Interestingly, surface melt (ME) shows a strong and significant positive correlation with SMB over 14-day cumulative periods ($r = 0.84$).

https://doi.org/10.5194/egusphere-2025-5562
Preprint. Discussion started: 17 February 2026

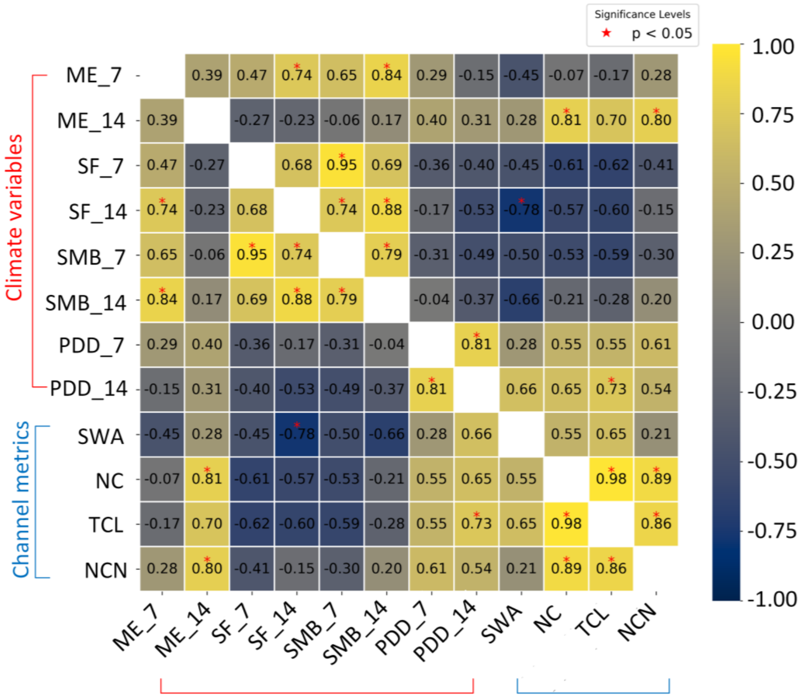

Figure 18: Linear relationships between climatic variables from MAR, ERA5 and seasonal key metrics of SCNs on Nivlisen Ice Shelf. Black numbers indicate the Pearson correlation coefficient. Climatic variables: ME-melt; SF-snowfall; SMB-surface mass balance; PDD-positive degree days. SCN metrics: SWA-surface water area; NC-number of channels; TCL- total channel length; NCN-number of channel networks. Variables calculated over fixed time windows (i.e., 7-day and 14-day) are denoted with subscripts '_7' and '_14'.

5 Discussion

5.1 Interannual evolution of SCNs

Over the eight-year record (2017-2024), SCNs on Nivlisen Ice Shelf exhibit pronounced interannual variability in their connectivity, extent, and structural complexity (Fig. 4). This study presents the first comprehensive, multi-year mapping and quantitative analysis of SCNs on Nivlisen Ice Shelf, revealing how SCNs alternate between highly integrated and fragmented states under varying climatic conditions. Despite these fluctuations, the main drainage network remained relatively stable in terms of its location, indicating that interannual variability primarily presents as changes in the degree of network connectivity rather than large-scale reorganisation of flow paths. When the ES, M and WS channels connected in 2019 and 2020, for example, the system exhibited its highest degree of connectivity, culminating in the formation of a large terminal lake near the ice front (Fig. 8). In contrast, no surface water was visible in Sentinel-2 optical imagery throughout the melt season of 2022. Instead, conditions on 25 January 2022

https://doi.org/10.5194/egusphere-2025-5562
Preprint. Discussion started: 17 February 2026

(Fig. 19c) show a uniformly bright ice shelf surface indicating fresh snow cover. In the subsequent melt season (2023), a modest recovery in surface water was observed, although channel length (Fig. 5) and depth (Fig. 6) remained limited. This partial recurrence may be linked to the presence of refrozen supraglacial channels that persisted through the winter and acted as conduits for new meltwater. Such a mechanism aligns with the findings from Dell et al. (2020), who proposed that relic meltwater channels, preserved as refrozen ice within the firn, can exert multiyear control over the surface meltwater routing and distribution. This idea is supported by Sentinel-1 Synthetic Aperture Radar (SAR) imagery acquired two days after the Sentinel-2 imagery (27 January 2022; Fig. 19d), which reveals a drainage network structure characterized by low-backscatter values (ranging from -15 to -25 dB) with spatial patterns closely matching those observed in 2020 (Fig. 19a-b). These backscatter values suggest the presence of meltwater concealed beneath a thin layer of snow or ice, or alternatively, water retained within a shallow, saturated firn layer (Dell et al., 2020). A similar phenomenon was reported on the Amery Ice Shelf by Spergel et al. (2021), where large-scale supraglacial lakes and extensive drainage networks were found to freeze completely in winter, as revealed by temporal changes in SAR backscatter. Importantly, such refrozen meltwater within channel networks forms impermeable ice layers that lie in channel depressions and which may promote extended surface pathways in later seasons, effectively generating a relatively 'stable' drainage configuration/network from year to year, albeit with differing amounts of meltwater present at the surface.

We find that surface topography is an important control on SCN development and direction on Nivlisen Ice Shelf. Channels are predominantly aligned with surface ice-flow stripes, producing a parallel pattern, reflecting the influence of long-term ice-flow morphology and internal stress regimes that constrain meltwater routing along pre-existing features (Glasser and Gudmundsson, 2012b; Chen et al., 2024). At a scale of 100's of meters to multiple kilometres, subtle surface rumples and slopes, particularly those associated with subglacial topographic pinning points or ice rises (cf. Miles and Bingham, 2024), redirect meltwater laterally and promote channel convergence. This is particularly observed in the substantial eastward diversion of the main WS channel (Fig. 14) by the raised ice surface (ice rise) above a basal pinning point. These observations demonstrate that even minor variations in surface slope can (re)organise SCNs and create spatial heterogeneity in meltwater routing. Ice surface topographic steering therefore defines the fundamental structure within which any liquid water moves and dictating where supraglacial channels form and persist across the ice shelf surface each year.

https://doi.org/10.5194/egusphere-2025-5562
Preprint. Discussion started: 17 February 2026

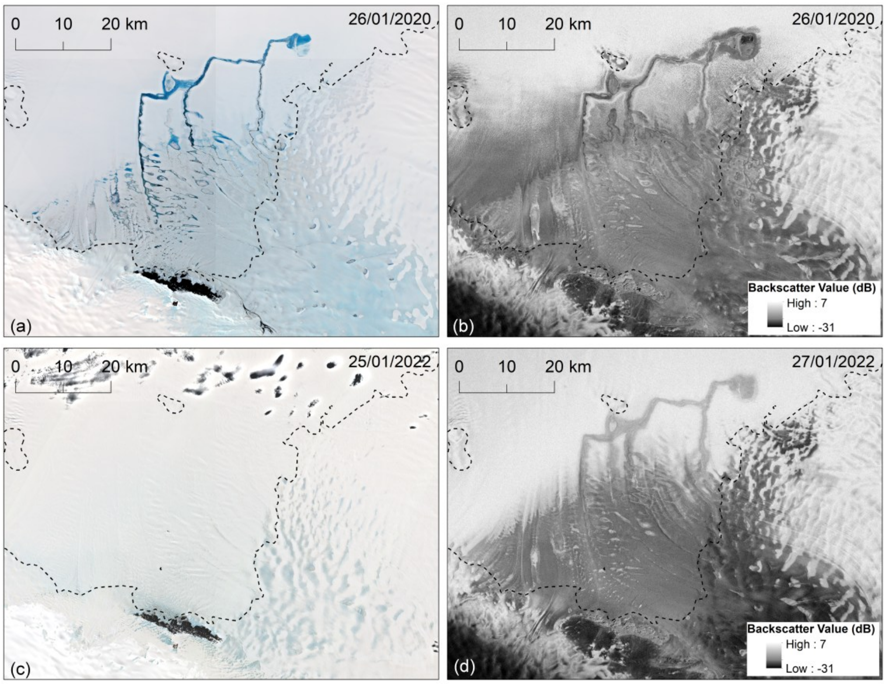

Figure 19: Comparison of supraglacial channel network observations on Nivlisen Ice Shelf from (a) and (c) Sentinel-2 optical imagery, (b) and (d) Sentinel-1 SAR imagery in January 2020 and 2022 respectively. The dashed black lines are grounding lines of Nivlisen Ice Shelf.

5.2 Seasonal evolution of SCNs

Beyond the importance of topography, climatic conditions must also be suitable for a significant network to form. A key characteristic of the surface drainage system on Nivlisen Ice Shelf is the progressive consolidation, and then fragmentation, of SCNs throughout the melt season. As the melt season advances, isolated and disconnected networks gradually merge into larger, more integrated systems, resulting in increased connectivity and more efficient water routing across the ice shelf surface. This seasonal reorganisation marks a transition from a fragmented early-season drainage configuration to a more stable and efficient surface network at peak melt. Although individual channels do not evolve at the same rate, the overall system becomes increasingly connected, optimising surface water flow and filling any channel-connected lakes. Importantly, despite the increased drainage efficiency, all the meltwater ultimately remains on the ice shelf in the time period of our observations, either retained within lakes or draining into the firn, indicating a closed surface hydrological system. These results align broadly with the seasonal patterns reported by Dirscherl et al. (2021), who used Sentinel-1 and Sentinel-2 observations to monitor supraglacial lakes across Antarctic ice shelves from 2015 to 2021. Both studies identify a peak in surface water coverage in January, followed by a rapid decline in February and near-complete

https://doi.org/10.5194/egusphere-2025-5562
Preprint. Discussion started: 17 February 2026

disappearance by March. The clustering of SCNs near the grounding line, is similar to the ponding identified on the Larsen C Ice Shelf (Bell et al., 2018; Lai et al., 2020).

The drainage system also evolves temporally. We particularly note that the water that was at higher elevations inland at the start of the melt season is less apparent as the season progresses and that this surface meltwater is progressively transferred from higher-elevation regions toward lower elevations near the shelf front over the melt season. The concurrent decrease in maximum elevation of surface water and increase in water depth during mid-season (Fig. 10) also indicates a transition toward more channelised, downslope flow. This suggests that channels in the higher part of the network that may have been slower-flowing and thus contained deeper water initially in the season, are able to evacuate water to the lower parts of the network more rapidly and thus have shallower water depths and are harder to identify in later imagery. Similar surface drainage evolution was observed by Kingslake et al. (2015) who documented a rapid, large-scale drainage event in 2007 when surface meltwater propagated more than 70 km from several high-elevation lakes near the grounding line toward the ice front, following refrozen pathways from previous years. Their modelling suggested that such 'unstable drainage' events occur when channels rapidly enlarge at lake outlets, allowing lakes to drain almost completely over the ice surface. However, our seasonal analysis indicates that the high-elevation source lakes identified by Kingslake et al. (2015) were not entirely emptied within a single melt season. Although these lakes briefly disappeared in early summer, they reappeared later in the season with smaller surface areas (see Fig.9), implying that partial refilling occurred. This behaviour does not contradict the unstable-drainage framework but rather reveals that surface drainage on Nivlisen can be very dynamic within a single melt season. The reappearance of lakes at higher elevations and close to the grounding line likely reflects their initial discharge and emptying, followed by renewed meltwater input later in the season. Similar cyclic behaviour has been observed on other Antarctic ice shelves, where early-season snow and firn initially inhibit surface ponding but later provide additional meltwater as they melt (Dell et al., 2020; Arthur et al., 2020, 2022). These processes indicate that the evolution of SCNs on Nivlisen is governed by feedback between meltwater supply, channel stability, and refreezing dynamics, resulting in a multi-phase drainage regime that differs from the single-event drainage predicted by idealised models.

In summary, our observations confirm that the SCNs on Nivlisen Ice Shelf redistribute meltwater across the shelf rather than exporting it off the ice shelf, consistent with widespread refreezing and firn infiltration at lower elevations. This behaviour is unlike grounded ice such as over Greenland and the Devon Ice Cap (Lu et al., 2020; Yang et al., 2021), where supraglacial drainage migrates upward through the season as new melt occurs at increasingly higher elevations. In such settings, rising equilibrium line altitudes and surface warming drive inland expansion of the ablation zone, while early-season meltwater at low elevations rapidly drains through moulins and crevasses. In contrast, the Nivlisen Ice Shelf exhibits a drainage system that does not expand inland and up-ice. Instead, it consists of a floating, 'closed' surface drainage system in which meltwater is redistributed toward lower elevations and retained through refreezing or ponding. These differences underscore the contrasting hydrological regimes between grounded and floating ice surfaces, particularly regarding connectivity, retention, and routing efficiency.

https://doi.org/10.5194/egusphere-2025-5562
Preprint. Discussion started: 17 February 2026

5.3 Climatic Controls on SCN evolution

Among the evaluated climatic drivers, mean summer temperature data from ERA5 showed the strongest and most consistent correlations with SCN metrics on an interannual scale (Fig. 16). Surface water area, the number of channel networks, the number of individual channels, and total channel length are all positively correlated with ERA5 temperatures ($r = 0.93$-0.99, $p < 0.05$), indicating that air temperature is the primary control on the extent of the SCN distribution on Nivlisen Ice Shelf. In contrast, *in-situ* temperature data from the nearby Novolazarevskaya Research Station has weaker correlations, particularly with total channel length ($r = 0.53$-0.67, $p > 0.05$). Correlations were statistically significant ($p < 0.05$) for all ERA5-based temperature-SCN relationships, whereas station-derived temperatures showed non-significant relationships ($p > 0.05$). This discrepancy likely reflects spatial representativeness: the station provides a limited 'point' measurement, while ERA5 data capture temperature variations across the ice shelf surface, better aligning with the spatial scale of SCN development. Correlations with snowfall and SMB were weaker and generally not statistically significant.

On a seasonal timescale, SCN metrics exhibit strong sensitivity to short-term cumulative temperature and melt indicators (Fig. 18). The 14-day surface melt (ME_14) and positive degree days (PDD_14) show significant positive correlations with the number of channels ($r = 0.81$) and total channel length ($r = 0.73$), highlighting the rapid response of surface drainage development to melt events and aligning with previous work (Kingslake et al., 2017; Dell et al., 2020). These relationships are statistically significant ($p < 0.05$) and indicate that supraglacial drainage responds within 1 to 2 weeks to cumulative melt energy increases. In contrast, snowfall (SF_14) is negatively but non-significant correlated with surface water area, likely due to the snowpack's ability to absorb or mask surface meltwater (Arthur et al., 2022). Surprisingly, surface melt (ME) also shows a strong positive correlation with SMB whereby more melt occurs when there is increased SMB. This relationship may arise from synchronous increases in melt and snowfall or may reflect the dominance of snowfall in the SMB budget under prevailing accumulation conditions (Dirscherl et al., 2021). It may also reflect that less energy is required to melt snow than it is to melt ice, so an abundance of snow simply provides a larger store of more rapidly accessible liquid water. SMB variability on Nivlisen Ice Shelf is therefore strongly dominated by accumulation: snowfall was also anomalously high during summers with enhanced melt, leading to net positive mass balance despite increased ablation. In such accumulation-dominated conditions, the magnitude of snowfall offsets the melt losses, producing a statistical coupling between ME and SMB (Donat-Magnin et al., 2021). Although this correlation is statistically significant ($r = 0.84$, $p < 0.05$), its physical interpretation remains complex, as both melt and SMB are strongly modulated by concurrent accumulation.

The interactions between climate and seasonal evolution of SCN appear more transient and immediate, whilst at an interannual timescale patterns reflect cumulative climatic influence over longer periods. At both timescales, only temperature-related variables show statistically significant correlations ($p < 0.05$),

https://doi.org/10.5194/egusphere-2025-5562
Preprint. Discussion started: 17 February 2026

reflecting their indirect and/or lagged influence. A recent study by Dirscherl et al. (2021) on the seasonal evolution of Antarctic supraglacial lakes from 2015 to 2021 further reinforces the importance of air temperature and solar radiation as primary climatic drivers of SGL on ice shelves around the EAIS. While their focus was on lake expansion and persistence, they identified positive correlations between surface temperature and lake area, which are consistent with our findings on channel network development. In contrast, Arthur et al. (2022) reported a weak positive but non-significant correlation between summer mean temperature and SGL volume ($R = 0.52$) on Nivlisen Ice Shelf, suggesting a relatively limited direct climatic influence. SGLs on Shackleton Ice Shelf in East Antarctica were also found to exhibit only a weak relationship with near-surface summer temperature ($R^2 = 0.15$, $p = 0.04$) (Arthur et al., 2020). Our correlation analyses based on temperature data from the ERA5 reanalysis demonstrate much higher correlations ($r > 0.9$, $p < 0.05$) between summer air temperatures and multiple key SCN metrics. This difference likely arises because channel networks respond more directly and rapidly to variations in meltwater flux than lakes (Dell et al., 2020). For example, total channel length or the number of channels as they evolve through a season tend to grow much more rapidly than lake area, and does so more instantaneously during a warm weather period. This is unsurprising because channels are enabling the filling of lakes, and thus channels evolve first and their initiation and integration are driven by local runoff and flow routing that react almost instantaneously to temperature-induced melt events (Kingslake et al., 2015). In contrast, lake expansion and contraction operate over longer timescales, constrained by basin topography and refreezing processes, which buffer their response to short-term climatic fluctuations (Banwell et al., 2021; Arthur et al., 2022). Moreover, the spatial distribution and connectivity of SCNs may be more sensitive to regional climate variations captured by the ERA5 reanalysis. The pronounced climatic sensitivities identified for SCNs also reflect their linear and interconnected morphology, which allows efficient meltwater delivery and rapid adjustment, especially where they are expanding along channels that existed in previous seasons. Compared with SGLs, where meltwater is stored and frequently refreezes, SCNs continuously transport meltwater across Nivlisen Ice Shelf. Their geometry and connectivity therefore make them more immediate and sensitive indicators of changes in meltwater supply and drainage efficiency.

Winter snowfall shows a weak negative correlation with annual SCN metrics, potentially due to its insulating effect reducing early season melt (Dell et al., 2020), or a firn retention effect whereby increased accumulation enhances firn air content and promotes meltwater storage and refreezing (Arthur et al., 2020, 2022). Meanwhile, spring and summer snowfall display weak positive correlations, possibly reflecting delayed snowmelt contributions to meltwater input. None of these correlations reach statistical significance ($p > 0.05$), implying that snowfall exerts an indirect rather than primary control, operating through surface albedo, insulation, and delayed meltwater release. The lack of strong correlation may result from competing effects: snow both inhibits and later contributes to surface melt (Dell et al., 2020; Arthur et al., 2022). Early-season snowfall increases surface albedo and limits energy absorption, thereby suppressing initial melt. Mid-season snow events can temporarily mask existing surface water and channels in optical imagery, as likely occurred in 2022. Later in the season, melting of accumulated snow adds additional water input to the drainage system. These opposing influences, insulation, masking, and

https://doi.org/10.5194/egusphere-2025-5562
Preprint. Discussion started: 17 February 2026

contribution, demonstrate that although the correlations are weak, the influence of snowfall and its timing have a dynamic impact both on the actual production of meltwater, its channelisation, and our ability to observe the SCNs at different times of the season.

6 Conclusions

This study provides a detailed characterisation of SCNs on Nivlisen Ice Shelf, focusing on their seasonal evolution and connectivity during the 2018-2019 melt season and interannual variability in January from 2017 to 2024. In total, we mapped 710 SCNs and 5513 channels on the Nivlisen over the 8-year period. By quantifying key metrics, including the water area, depth, number of channels and number of SCNs, we show high interannual variability (>100 %) in surface drainage networks across Nivlisen Ice Shelf, with the interannual evolution showing a general pattern of expansion, peak development, and substantial decline. In the summer of 2018, surface water extent peaked, with 1650 channels organised into 186 drainage networks, and a total channel length of approximately 1440 km. Seasonally, during the summer of 2018-2019 surface meltwater was efficiently delivered from high-elevation (about 400 m) lakes to low elevations (50 m) near the ice front through 924 channels with total length of 967 km. The SCNs exhibited a dynamic process characterized by initial isolated appearance of surface water bodies near the grounding line, followed by expansion, peak connectivity, and finally, fragmentation as meltwater refreezes. As the connectivity evolves through a season, it enables the area covered by SCNs to expand across the ice shelf but at the same time, it means the channels which initially formed near the grounding line more efficiently transport water into the lower channel network, thus contain shallower water and are not visible in the imagery. Hence, the system evolves from a less efficient to more efficient system over the melt season, transporting meltwater to lower regions of the ice shelf.

Relationships between seasonal hydrological metrics and climatic drivers from the MAR climate model and ERA5 reanalysis reveal the sensitivity of SCNs to both seasonal and interannual temperature variability, confirming temperature as a primary driver controlling the extent, connectivity, and structural evolution of surface drainage systems. In addition, our work suggests that there are complexities relating to the influence of snowfall on the development and/or observation of the network and that these depend on the time of year in which snowfall is deposited and how readily it can be melted. The observed increase in connectivity and routing efficiency implies that meltwater can be redistributed over large areas of the ice shelf during warm summers and that this routing is linked to the structure of the ice shelf (e.g. crevasses and flow stripes) as well as ice surface undulations at a range of scales which act to steer water flow. This creates the framework for a drainage network that is reoccupied each year, but to varying degrees based on the complex relationship between melt and snowfall. In particular, the presence of a topographic pinning point acts to reverse ice surface gradients and thus divert the main drainage channels at nearly right-angles resulting in a flow-transverse channel that cross-cuts and thus captures the three main channel outlets, feeding water into a major supraglacial lake. By linking detailed observations of SCN evolution with climatic forcing, this work provides crucial insights into how surface meltwater is

https://doi.org/10.5194/egusphere-2025-5562
Preprint. Discussion started: 17 February 2026

potentially delivered within the surface drainage system of an ice shelf, a process with increasingly important implications for the surface mass balance and overall stability of the AIS in a warming future.

7 Appendices

Table A1: Sentinel-2 and Landsat-8 imagery information

Data type	Spatial Resolution	Number or Row/Path	Acquisition Date
Sentinel 2	10 m	R049_T32DNG	2017/01/26
		R049_T32DNH	
		R049_T32DPG	
		R049_T32DPH	
		R049_T32DNG	2018/01/11
		R049_T32DNH	
		R049_T32DPG	
		R049_T32DPH	
		R049_T32DNG	2019/01/31
		R049_T32DNH	
		R049_T32DPG	
		R049_T32DPH	
		R049_T32DNG	2020/01/26
		R049_T32DNH	
		R049_T32DPG	
		R049_T32DPH	
		R049_T32DNG	2021/01/20
		R049_T32DNH	
		R049_T32DPG	
		R049_T32DPH	
		R049_T32DNG	2022/01/25
		R049_T32DNH	
		R049_T32DPG	
		R049_T32DPH	
		R006_T32DNG	2023/01/27
		R006_T32DNH	
		R006_T32DPG	
		R006_T32DPH	

https://doi.org/10.5194/egusphere-2025-5562
Preprint. Discussion started: 17 February 2026

		R006_T32DNG R006_T32DNH R006_T32DPG R006_T32DPH	2024/01/22
Landsat 8	30 m	110/166	2018/12/01
		110/165	2018/12/10
		110/166	2018/12/17
		109/167	2018/12/24
		110/167	2018/12/24
		109/167	2019/01/25
		110/167	2019/01/25
		110/166	2019/02/19
		110/165	2019/02/28
		110/166	2019/03/07

Data availability

The satellite imagery, REMA DEM, and meteorological data are all open access and freely available (ref. Section 3 Data and methods). The supraglacial channel networks mapped in this study is available upon request from the corresponding author (Jiao Chen: jiao.chen@durham.ac.uk)

Authors contributions

All authors contributed to the conceptualisation of this project. JC conducted the mapping and data analysis under the supervision of RAH, SSRJ and CRS. JC led manuscript writing with comments and revisions provided by all authors.

Competing interests

The corresponding author has declared that none of the authors has any competing interests.

Acknowledgements

This work was supported by China Scholarship Council - Durham University joint scholarship held by Jiao Chen (grant reference CSC No. 202208890014).

https://doi.org/10.5194/egusphere-2025-5562
Preprint. Discussion started: 17 February 2026

8 References

Alley, K. E., Scambos, T. A., Miller, J. Z., Long, D. G., and MacFerrin, M.: Quantifying vulnerability of Antarctic ice shelves to hydrofracture using microwave scattering properties, Remote Sensing of Environment, 210, 297–306, https://doi.org/10.1016/j.rse.2018.03.025, 2018.

Arthur, J. F., Stokes, C. R., Jamieson, S. S. R., Carr, J. R., and Leeson, A. A.: Distribution and seasonal evolution of supraglacial lakes on Shackleton Ice Shelf, East Antarctica, The Cryosphere, 14, 4103–4120, https://doi.org/10.5194/tc-14-4103-2020, 2020.

Arthur, J. F., Stokes, C. R., Jamieson, S. S. R., Rachel Carr, J., Leeson, A. A., and Verjans, V.: Large interannual variability in supraglacial lakes around East Antarctica, Nat Commun, 13, 1711, https://doi.org/10.1038/s41467-022-29385-3, 2022.

Banwell, A. F., MacAyeal, D. R., and Sergienko, O. V.: Breakup of the Larsen B Ice Shelf triggered by chain reaction drainage of supraglacial lakes: LARSEN B CHAIN REACTION LAKE DRAINAGE, Geophys. Res. Lett., 40, 5872–5876, https://doi.org/10.1002/2013GL057694, 2013.

Banwell, A. F., Caballero, M., Arnold, N. S., Glasser, N. F., Mac Cathles, L., and MacAyeal, D. R.: Supraglacial lakes on the Larsen B ice shelf, Antarctica, and at Paakitsoq, West Greenland: a comparative study, Ann. Glaciol., 55, 1–8, https://doi.org/10.3189/2014AoG66A049, 2014.

Banwell, A. F., Datta, R. T., Dell, R. L., Moussavi, M., Brucker, L., Picard, G., Shuman, C. A., and Stevens, L. A.: The 32-year record-high surface melt in 2019/2020 on the northern George VI Ice Shelf, Antarctic Peninsula, The Cryosphere, 15, 909–925, https://doi.org/10.5194/tc-15-909-2021, 2021.

Bell, R. E., Chu, W., Kingslake, J., Das, I., Tedesco, M., Tinto, K. J., Zappa, C. J., Frezzotti, M., Boghosian, A., and Lee, W. S.: Antarctic ice shelf potentially stabilized by export of meltwater in surface river, Nature, 544, 344–348, https://doi.org/10.1038/nature22048, 2017.

Bell, R. E., Banwell, A. F., Trusel, L. D., and Kingslake, J.: Antarctic surface hydrology and impacts on ice-sheet mass balance, Nature Clim Change, 8, 1044–1052, https://doi.org/10.1038/s41558-018-0326-3, 2018.

Berger, S., Favier, L., Drews, R., Derwael, J.-J., and Pattyn, F.: The control of an uncharted pinning point on the flow of an Antarctic ice shelf, J. Glaciol., 62, 37–45, https://doi.org/10.1017/jog.2016.7, 2016.

Chandler, D. M. and Hubbard, A.: Widespread partial-depth hydrofractures in ice sheets driven by supraglacial streams, Nat. Geosci., https://doi.org/10.1038/s41561-023-01208-0, 2023.

Chen, J., Hodge, R. A., Jamieson, S. S. R., and Stokes, C. R.: Distribution and Morphometry of Large Supraglacial Channels on Five Antarctic Ice Shelves, J. Glaciol., 1–53, https://doi.org/10.1017/jog.2024.99, 2024.

Corr, D., Leeson, A., McMillan, M., Zhang, C., and Barnes, T.: An inventory of supraglacial lakes and channels across the West Antarctic Ice Sheet, Earth Syst. Sci. Data, 14, 209–228, https://doi.org/10.5194/essd-14-209-2022, 2022.

Dell, R., Arnold, N., Willis, I., Banwell, A., Williamson, A., Pritchard, H., and Orr, A.: Lateral meltwater transfer across an Antarctic ice shelf, The Cryosphere, 14, 2313–2330, https://doi.org/10.5194/tc-14-2313-2020, 2020.

Dirscherl, M. C., Dietz, A. J., and Kuenzer, C.: Seasonal evolution of Antarctic supraglacial lakes in 2015–2021 and links to environmental controls, The Cryosphere, 15, 5205–5226, https://doi.org/10.5194/tc-15-5205-2021, 2021.

Donat-Magnin, M., Jourdain, N. C., Kittel, C., Agosta, C., Amory, C., Gallée, H., Krinner, G., and Chekki, M.: Future surface mass balance and surface melt in the Amundsen sector of the West Antarctic Ice Sheet, The Cryosphere, 15, 571–593, https://doi.org/10.5194/tc-15-571-2021, 2021.

Dunmire, D., Lenaerts, J. T. M., Banwell, A. F., Wever, N., Shragge, J., Lhermitte, S., Drews, R., Pattyn, F., Hansen, J. S. S., Willis, I. C., Miller, J., and Keenan, E.: Observations of Buried Lake Drainage on the Antarctic Ice Sheet, Geophysical Research Letters, 47, e2020GL087970, https://doi.org/10.1029/2020GL087970, 2020.

Fretwell, P., Pritchard, H., Vaughan, D., Bamber, J., Barrand, N., Bell, R. E., Bianchi, C., Bingham, R., Blankenship, D., Casassa, G., Catania, G., Callens, D., Conway, H., Cook, A., Corr, H., Damaske, D., Damn, V., Ferraccioli, F., Forsberg, R., Fujita, S., Gim, Y., Gogineni, P., Griggs, J., Hindmarsh, R., Holmlund, P., Holt, J. W., Jacobel, R., Jenkins, A., Jokat, W., Jordan, T., King, E., Kohler, J., Krabill, W., Riger-Kusk, M., Langley, K., Leitchenkov, G., Leuschen, C., Luyendyk, B., Matsuoka, K., Mouginot, J., Nitsche, F., Nogi, Y., Nost, O., Popov, S., Rignot, E., Rippin, D., Rivera, A., Roberts, J. L., Ross, N., Siegert, M., Smith, A., Steinhage, D., Studinger, M., Sun, B., Tinto, K., Welch, B., Wilson, D. S., Young, D., Xiangbin, C., and Zirizzotti, A.: BEDMAP2 - Ice thickness, bed and surface elevation for Antarctica - gridding products (1.0), https://doi.org/10.5285/FA5D606C-DC95-47EE-9016-7A82E446F2F2, 2022.

Glasser, N. F. and Gudmundsson, G. H.: Longitudinal surface structures (flowstripes) on Antarctic glaciers, The Cryosphere, 6, 383–391, https://doi.org/10.5194/tc-6-383-2012, 2012a.

Glasser, N. F. and Gudmundsson, G. H.: Longitudinal surface structures (flowstripes) on Antarctic glaciers, The Cryosphere, 6, 383–391, https://doi.org/10.5194/tc-6-383-2012, 2012b.

Glen, E., Banwell, A., Maddalena, J., Leeson, A., Corr, D., and McMillan, M.: A comparison of supraglacial lake characteristics and drainage dynamics in Southwest Greenland between an extreme high, and an extreme low, melt season, display, https://doi.org/10.5194/egusphere-egu22-7675, 2022.

Glen, E., Leeson, A., Banwell, A. F., Maddalena, J., Corr, D., Atkins, O., Noël, B., and McMillan, M.: A comparison of supraglacial meltwater features throughout contrasting melt seasons: southwest Greenland, The Cryosphere, 19, 1047–1066, https://doi.org/10.5194/tc-19-1047-2025, 2025.

Hanna, E., Topál, D., Box, J. E., Buzzard, S., Christie, F. D. W., Hvidberg, C., Morlighem, M., De Santis, L., Silvano, A., Colleoni, F., Sasgen, I., Banwell, A. F., Van Den Broeke, M. R., DeConto, R., De Rydt, J., Goelzer, H., Gossart, A., Gudmundsson, G. H., Lindbäck, K., Miles, B., Mottram, R., Pattyn, F., Reese, R., Rignot, E., Srivastava, A., Sun, S., Toller, J., Tuckett, P. A., and Ultee, L.: Short- and long-term variability of the Antarctic and Greenland ice sheets, Nat Rev Earth Environ, 5, 193–210, https://doi.org/10.1038/s43017-023-00509-7, 2024.

Harris Geospatial Solutions: ENVI 5.6 Help, 2020.

He, L., Ren, X., Gao, Q., Zhao, X., Yao, B., and Chao, Y.: The connected-component labeling problem: A review of state-of-the-art algorithms, Pattern Recognition, 70, 25–43, https://doi.org/10.1016/j.patcog.2017.04.018, 2017.

Hersbach, H., Bell, B., Berrisford, P., Hirahara, S., Horányi, A., Muñoz-Sabater, J., Nicolas, J., Peubey, C., Radu, R., Schepers, D., Simmons, A., Soci, C., Abdalla, S., Abellan, X., Balsamo, G., Bechtold, P., Biavati, G., Bidlot, J., Bonavita, M., De Chiara, G., Dahlgren, P., Dee, D., Diamantakis, M., Dragani, R., Flemming, J., Forbes, R., Fuentes, M., Geer, A., Haimberger, L., Healy, S., Hogan, R. J., Hólm, E., Janisková, M., Keeley, S., Laloyaux, P., Lopez, P., Lupu, C., Radnoti, G., De Rosnay, P., Rozum, I., Vamborg, F., Villaume, S., and Thépaut, J.: The ERA5 global reanalysis, Quart J Royal Meteoro Soc, 146, 1999–2049, https://doi.org/10.1002/qj.3803, 2020.

Howat, I. M., Porter, C., Smith, B. E., Noh, M.-J., and Morin, P.: The Reference Elevation Model of Antarctica, The Cryosphere, 13, 665–674, https://doi.org/10.5194/tc-13-665-2019, 2019.

https://doi.org/10.5194/egusphere-2025-5562
Preprint. Discussion started: 17 February 2026

Hui, F., Ci, T., Cheng, X., Scambo, T. A., Liu, Y., Zhang, Y., Chi, Z., Huang, H., Wang, X., Wang, F., Zhao, C., Jin, Z., and Wang, K.: Mapping blue-ice areas in Antarctica using ETM+ and MODIS data, Ann. Glaciol., 55, 129–137, https://doi.org/10.3189/2014AoG66A069, 2014.

Kingslake, J., Ng, F., and Sole, A.: Modelling channelized surface drainage of supraglacial lakes, J. Glaciol., 61, 185–199, https://doi.org/10.3189/2015JoG14J158, 2015.

Kingslake, J., Ely, J. C., Das, I., and Bell, R. E.: Widespread movement of meltwater onto and across Antarctic ice shelves, Nature, 544, 349–352, https://doi.org/10.1038/nature22049, 2017.

Kittel, C., Amory, C., Agosta, C., Jourdain, N. C., Hofer, S., Delhasse, A., Doutreloup, S., Huot, P.-V., Lang, C., Fichefet, T., and Fettweis, X.: Diverging future surface mass balance between the Antarctic ice shelves and grounded ice sheet, The Cryosphere, 15, 1215–1236, https://doi.org/10.5194/tc-15-1215-2021, 2021.

Lai, C.-Y., Kingslake, J., Wearing, M. G., Chen, P.-H. C., Gentine, P., Li, H., Spergel, J. J., and Van Wessem, J. M.: Vulnerability of Antarctica's ice shelves to meltwater-driven fracture, Nature, 584, 574–578, https://doi.org/10.1038/s41586-020-2627-8, 2020.

Langley, E. S., Leeson, A. A., Stokes, C. R., and Jamieson, S. S. R.: Seasonal evolution of supraglacial lakes on an East Antarctic outlet glacier, Geophys. Res. Lett., 43, 8563–8571, https://doi.org/10.1002/2016GL069511, 2016.

Lenaerts, J. T. M., Lhermitte, S., Drews, R., Ligtenberg, S. R. M., Berger, S., Helm, V., Smeets, C. J. P. P., Broeke, M. R. van den, van de Berg, W. J., van Meijgaard, E., Eijkelboom, M., Eisen, O., and Pattyn, F.: Meltwater produced by wind–albedo interaction stored in an East Antarctic ice shelf, Nature Clim Change, 7, 58–62, https://doi.org/10.1038/nclimate3180, 2017.

Lindbäck, K., Moholdt, G., Nicholls, K. W., Hattermann, T., Pratap, B., Thamban, M., and Matsuoka, K.: Spatial and temporal variations in basal melting at Nivlisen ice shelf, East Antarctica, derived from phase-sensitive radars, The Cryosphere, 13, 2579–2595, https://doi.org/10.5194/tc-13-2579-2019, 2019.

Lu, Y., Yang, K., Lu, X., Smith, L. C., Sole, A. J., Livingstone, S. J., Fettweis, X., and Li, M.: Diverse supraglacial drainage patterns on the Devon ice Cap, Arctic Canada, Journal of Maps, 16, 834–846, https://doi.org/10.1080/17445647.2020.1838353, 2020.

Melling, L., Leeson, A., McMillan, M., Maddalena, J., Bowling, J., Glen, E., Sandberg Sørensen, L., Winstrup, M., and Lørup Arildsen, R.: Evaluation of satellite methods for estimating supraglacial lake depth in southwest Greenland, The Cryosphere, 18, 543–558, https://doi.org/10.5194/tc-18-543-2024, 2024.Miles, B. and Bingham, R.: Antarctic ice shelf pinning point change classification 1973-2022, https://doi.org/10.7488/DS/7583, 2023.

Miles, B. W. J. and Bingham, R. G.: Progressive unanchoring of Antarctic ice shelves since 1973, Nature, 626, 785–791, https://doi.org/10.1038/s41586-024-07049-0, 2024.

Mouginot, J., Scheuchl, B., and Rignot, E.: MEaSUREs Antarctic Boundaries for IPY 2007-2009 from Satellite Radar, Version 2, https://doi.org/10.5067/AXE4121732AD, 2017.

Moussavi, M., Pope, A., Halberstadt, A., Trusel, L., Cioffi, L., and Abdalati, W.: Antarctic Supraglacial Lake Detection Using Landsat 8 and Sentinel-2 Imagery: Towards Continental Generation of Lake Volumes, Remote Sensing, 12, 134, https://doi.org/10.3390/rs12010134, 2020.

Moussavi, M. S., Abdalati, W., Pope, A., Scambos, T., Tedesco, M., MacFerrin, M., and Grigsby, S.: Derivation and validation of supraglacial lake volumes on the Greenland Ice Sheet from high-resolution satellite imagery, Remote Sensing of Environment, 183, 294–303, https://doi.org/10.1016/j.rse.2016.05.024, 2016.

https://doi.org/10.5194/egusphere-2025-5562
Preprint. Discussion started: 17 February 2026

National Research Council (U.S.): Future science opportunities in Antarctica and the southern ocean, Online-Ausg., National Academies Press, Washington, D.C, 195 pp., 2011.

Ostertagová, E., Ostertag, O., and Kováč, J.: Methodology and Application of the Kruskal-Wallis Test, AMM, 611, 115–120, https://doi.org/10.4028/www.scientific.net/AMM.611.115, 2014.

Pitcher, L. H. and Smith, L. C.: Supraglacial Streams and Rivers, Annu. Rev. Earth Planet. Sci., 47, 421–452, https://doi.org/10.1146/annurev-earth-053018-060212, 2019.

Pope, A., Scambos, T. A., Moussavi, M., Tedesco, M., Willis, M., Shean, D., and Grigsby, S.: Estimating supraglacial lake depth in West Greenland using Landsat 8 and comparison with other multispectral methods, The Cryosphere, 10, 15–27, https://doi.org/10.5194/tc-10-15-2016, 2016.

Spergel, J. J., Kingslake, J., Creyts, T., Van Wessem, M., and Fricker, H. A.: Surface meltwater drainage and ponding on Amery Ice Shelf, East Antarctica, 1973–2019, J. Glaciol., 67, 985–998, https://doi.org/10.1017/jog.2021.46, 2021.

Stokes, C. R., Sanderson, J. E., Miles, B. W. J., Jamieson, S. S. R., and Leeson, A. A.: Widespread distribution of supraglacial lakes around the margin of the East Antarctic Ice Sheet, Sci Rep, 9, 13823, https://doi.org/10.1038/s41598-019-50343-5, 2019.

Tuckett, P. A., Ely, J. C., Sole, A. J., Lea, J. M., Livingstone, S. J., Jones, J. M., and Van Wessem, J. M.: Automated mapping of the seasonal evolution of surface meltwater and its links to climate on the Amery Ice Shelf, Antarctica, The Cryosphere, 15, 5785–5804, https://doi.org/10.5194/tc-15-5785-2021, 2021.

Tuckett, P. A., Sole, A. J., Livingstone, S. J., Jones, J. M., Lea, J. M., and Gilbert, E.: Continent-wide mapping shows increasing sensitivity of East Antarctica to meltwater ponding, Nat. Clim. Chang., 15, 775–783, https://doi.org/10.1038/s41558-025-02363-5, 2025.

Turner, J., Colwell, S. R., Marshall, G. J., Lachlan-Cope, T. A., Carleton, A. M., Jones, P. D., Lagun, V., Reid, P. A., and Iagovkina, S.: The SCAR READER Project: Toward a High-Quality Database of Mean Antarctic Meteorological Observations, J. Climate, 17, 2890–2898, https://doi.org/10.1175/1520-0442(2004)017%253C2890:TSRPTA%253E2.0.CO;2, 2004.

Van Der Veen, C. J.: Fracture propagation as means of rapidly transferring surface meltwater to the base of glaciers, Geophysical Research Letters, 34, 2006GL028385, https://doi.org/10.1029/2006GL028385, 2007.

Vandecrux, B., Fausto, R. S., Van As, D., Colgan, W., Langen, P. L., Haubner, K., Ingeman-Nielsen, T., Heilig, A., Stevens, C. M., MacFerrin, M., Niwano, M., Steffen, K., and Box, J. E.: Firn cold content evolution at nine sites on the Greenland ice sheet between 1998 and 2017, J. Glaciol., 66, 591–602, https://doi.org/10.1017/jog.2020.30, 2020.

Williamson, A. G., Banwell, A. F., Willis, I. C., and Arnold, N. S.: Dual-satellite (Sentinel-2 and Landsat 8) remote sensing of supraglacial lakes in Greenland, The Cryosphere, 12, 3045–3065, https://doi.org/10.5194/tc-12-3045-2018, 2018.

Yang, K., Smith, L. C., Chu, V. W., Pitcher, L. H., Gleason, C. J., Rennermalm, A. K., and Li, M.: Fluvial morphometry of supraglacial river networks on the southwest Greenland Ice Sheet, GIScience & Remote Sensing, 53, 459–482, https://doi.org/10.1080/15481603.2016.1162345, 2016.

Yang, K., Smith, L. C., Cooper, M. G., Pitcher, L. H., Van As, D., Lu, Y., Lu, X., and Li, M.: Seasonal evolution of supraglacial lakes and rivers on the southwest Greenland Ice Sheet, J. Glaciol., 67, 592–602, https://doi.org/10.1017/jog.2021.10, 2021.

Zhang, W., Yang, K., Smith, L. C., Wang, Y., Van As, D., Noël, B., Lu, Y., and Liu, J.: Pan-Greenland mapping of supraglacial rivers, lakes, and water-filled crevasses in a cool summer (2018) and a warm

https://doi.org/10.5194/egusphere-2025-5562
Preprint. Discussion started: 17 February 2026

summer (2019), Remote Sensing of Environment, 297, 113781, https://doi.org/10.1016/j.rse.2023.113781, 2023.